Electron spectroscopies for Ce compounds in the impurity model

O. Gunnarsson
Max-Planck-Institut für Festkörperforschung, D-7000 Stuttgart, West Germany

K. Schönhammer
I. Institut für Theoretische Physik, Universität Hamburg, D-2000 Hamburg, West Germany

(Received 4 May 1983)

We present a method for calculating the core-level x-ray photoemission (XPS), the $3d \rightarrow 4f$ x-ray absorption (XAS), the valence photoemission, and the bremsstrahlung isochromat spectra in a slightly modified Anderson impurity model of a Ce compound at zero temperature. Both the spin and orbital degeneracies of the f level are included and the Coulomb interaction between the f electrons is taken into account. The spectra are expressed in terms of a resolvent operator. A many-electron basis set is introduced, and the resolvent is obtained from a matrix inversion. The particular form of the Anderson model allows us to find a small but sufficiently complete basis set, if the degeneracy N_f of the f level is large. In particular, we consider the limit $N_f \rightarrow \infty$, and show that the method is exact for the XPS, XAS, and valence photoemission spectra in this limit. It is also demonstrated that for $N_f \gtrsim 6$, the method provides accurate spectra. Analytical results are obtained for the valence photoemission spectrum $\rho_v(\epsilon)$. The spectrum has a sharp rise close to the Fermi energy ϵ_F, which goes over to a "Kondo peak" in the spin-fluctuation limit. An exact relation between $\rho_v(\epsilon_F)$ and the f-level occupancy n_f is shown to be satisfied to within 10% for $N_f \geq 6$. We discuss how core-level XPS spectra can be used to estimate the f-level occupancy n_f and the coupling Δ between the f level and the conduction states. We find that the values of n_f and Δ obtained from core-level XPS are basically consistent with the other spectroscopies and the static, $T=0$ susceptibility. It is, therefore, possible to describe these experiments in the Anderson model, using essentially the same set of parameters for all the experiments. Typically, we find $n_f > 0.7$ and $\Delta \sim 0.1$ eV.

I. INTRODUCTION

The aim of this paper is to present a simple but accurate method for calculating the core and valence photoemission, the $3d \rightarrow 4f$ x-ray absorption, and the bremsstrahlung isochromat spectra of Ce compounds. These systems have many unusual properties due to the presence of a $4f$ electron which shows both localized and itinerant behaviour.[1-3] Much of the discussion has therefore focused on the properties of the $4f$ level, in particular its occupancy n_f and coupling Δ to the conduction states.

There have been numerous studies of thermodynamic and transport properties,[1-3] such as the lattice parameter, the susceptibility, the specific heat, the resistivity, and the quasielastic linewidth in neutron scattering. From these experiments, sometimes referred to as "low-energy" or "slow" experiments, it has been concluded that $\Delta \sim 0.01$ eV and that, depending on the system, n_f can take any value between 0 and 1.[1-6] Such experiments, however, give fairly indirect information about n_f and Δ and a quantitative evaluation of these properties is difficult.

In particular, in the last few years, there have been many electron-spectroscopy measurements, so-called "high-energy" experiments, such as core level x-ray-photoemission (XPS),[7-10] valence-photoemission,[10-13] x-ray-absorption (XAS),[8,14,15] and bremsstrahlung isochromat (BIS) spectroscopy.[16] These electron spectroscopies also give rather indirect information about n_f and Δ. However, there are many indications from these experiments that Δ is substantially larger than 0.01 eV and that n_f is never close to zero. Large values of n_f have also been deduced from Compton scattering[17] and positron-annihilation[18] experiments.

In this paper we present a theory at $T=0$ for the electron spectroscopies mentioned above. We discuss the general properties of the spectra and to what extent quantitative results for n_f and Δ can be obtained. We find values of Δ which are typically 1 order of magnitude larger than those deduced from the low-energy experiments. For n_f we obtain values larger than about 0.7. In view of this large discrepancy to the results obtained from the low-energy experiments, we study the $T=0$ susceptibility data and the lattice-parameter results. We find that the susceptibility data are consistent with the new values of n_f and Δ and that the lattice-parameter data are not necessarily in conflict with these new values.

Much of the theoretical discussion of Ce compounds has been based on the Anderson (single-impurity) model[19] where one considers the f level on one atom and its interaction with the conduction states. Effects due to the (indirect) interaction between f levels on different atoms are neglected. While this interaction is obviously crucial for certain properties, for instance, magnetic ordering, the model seems to describe other properties successfully. Physical effects neglected in the model can be partly accounted for by the use of renormalized parameters. Since the renormalization may be different for different experiments the model gains credibility and usefulness if it can

 ©1983 The American Physical Society

describe different experiments with the same parameters. In this paper we therefore develop a theory for several experiments, and indicate that the Anderson model with essentially unchanged parameters can describe these experiments. A more detailed comparison with experiment is presented elsewhere.[20–23]

Since the coupling Δ between the f level and the conduction states is weak, it is useful to consider the states when $\Delta=0$. This is shown schematically in Fig. 1, where for *this* discussion we have replaced the conduction band by a single (degenerate) level. Although this is an oversimplification, some important features of the core spectroscopies can be illustrated. The levels of Fig. 1 are classified according to the number of f electrons. The creation of a core hole leads to a dramatic reordering in energy of the configurations due to the strong Coulomb interaction between the core hole and an f electron (see Fig. 1). It is crucial to include this interaction in the model.

We now use Fig. 1 to discuss core-level XPS since this spectroscopy is particularly useful for the determination of n_f and Δ. In the sudden approximation the XPS current is directly related to the core spectral function

$$\rho_c(\epsilon)=\sum_n |\langle E_n(N-1)|\psi_c|\phi_0\rangle|^2 \times\delta(\epsilon-E_0(N)+E_n(N-1)) , \quad (1.1)$$

where $|\phi_0\rangle$ is the ground state, $|E_n(N-1)\rangle$ are the excited states (final states) in the presence of a core hole and $E_0(N)$, and $E_n(N-1)$ are the corresponding energies. The annihilation operator for the core level is ψ_c. To evaluate this expression we write the initial ground state of Fig. 1 for nonzero Δ as

$$|\phi_0\rangle=c_0|f^0\rangle+c_1|f^1\rangle+c_2|f^2\rangle , \quad (1.2)$$

with obvious notations. It is usually assumed that the coupling between the states is much smaller than the f^1-f^2 energy separation so that $c_2\approx 0$. In the same spirit, one may assume that each final state $|E_n(N-1)\rangle$ is a pure f configuration, i.e., the final states are $|f^0\rangle$, $|f^1\rangle$, and $|f^2\rangle$. If $c_2=0$ only the first two states would couple to $|\phi_0\rangle$ and the corresponding peaks in the spectrum would have the weights $|c_0|^2$ and $|c_1|^2$; we could therefore read off the value of n_f from the weight of the f^1 peak of the core spectrum. For most Ce compounds, however, the core spectrum also shows a shoulder due to final states of mainly f^2 character.[7–10] This is only possible if there is a mixing of the f^1 and f^2 configurations in the initial and/or final states so that the f^2-like final state couples to the initial state. A mixing of the final-state configuration means that calculations are needed to determine to what extent n_f can be obtained from a core spectrum. The weight of the f^2 shoulder provides a measure of this mixing from which one can deduce the size of Δ. While Δ is large enough to couple the f^1 and f^2 configurations the calculations show that the mixing of the final f^0 and f^1 configurations, which have a larger energy separation, is fairly small. The weight of the f^0 peak therefore provides a semiquantitative measure of $|c_0|^2\approx 1-n_f$ and quantitative estimates can be obtained from the calculations. We have used these ideas extensively to estimate n_f and Δ for many La and Ce compounds.[21]

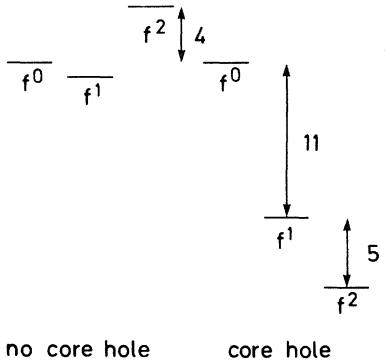

FIG. 1. Schematic representation of the energies of different configurations of a Ce impurity without and with a core hole. Configurations are labeled according to the number of f electrons. Typical energy differences (Refs. 7–10, 24, and 25) are indicated (in eV).

As emphasized above, it is important to include the interaction between a core hole and the f level. There have been many calculations[26,27] of the core spectrum for models including the attraction of a core hole on a valence level.[28] Usually, however, the valence level was assumed to be nondegenerate and the interaction between the valence electrons was therefore neglected. The calculation of the core spectrum is then equivalent to solving a time-dependent one-particle problem.[29] For a Ce compound the large degeneracy N_f of the f level is important, and to treat the f^2 shoulder in the XPS core spectrum, for instance, one at least needs to take the spin degeneracy ($N_f=2$) into account. Because of the strong Coulomb interaction between the f electrons, correlation then becomes very important and the calculation of the core spectrum is a true many-body problem. Recently, Oh and Doniach[30] proposed a Green's-function decoupling technique for calculating the core spectrum of a spin-degenerate model taking correlation effects into account. Their decoupling scheme provides an approximate description in the limit of a small coupling Δ, but from their calculations they inferred that to describe Ce compounds one cannot use a very small Δ. It turns out that for the interesting parameters their scheme breaks down, shown by the presence of energy regions with *negative* spectral weight.

An important progress in the treatment of the Anderson model, was the realization by Ramakrishnan[31] and Anderson[31] that for the calculation of the thermodynamic properties there is a small parameter $1/N_f$, where N_f is the degeneracy of the f level. We show that similar ideas can be applied to the spectroscopies. The calculation of the core and valence photoemission spectra is therefore greatly simplified if N_f is increased from 2 (spin degeneracy) to 14 (spin and orbital degeneracy), although, as indicated above, the step of N_f from 1 to 2 is a severe complication.

For the spectroscopies considered here, the measured quantity can be related to an expectation value of the resolvent operator $[z-E_0(N)+H]^{-1}$,

$$g(z)=\left\langle \phi_0 \left| T^{\dagger} \frac{1}{z-E_0(N)+H} T \right| \phi_0 \right\rangle . \tag{1.3}$$

The core spectral function for instance, is given by

$$\rho_c(\epsilon)=\mathrm{Im}g(\epsilon-i0^+)/\pi$$

if $T=\psi_c$. We now introduce a set of many-electron basis functions $|i\rangle$ and assume that the set is approximately complete. Inserting the unit operator $1\approx\sum |i\rangle\langle i|$ on both sides of $[z-E_0(N)+H]^{-1}$ in (1.3) gives

$$g(z)=\sum_{i,j} \langle \phi_0 | T^{\dagger} | i \rangle \left\langle i \left| \frac{1}{z-E_0(N)+H} \right| j \right\rangle \langle j | T | \phi_0 \rangle . \tag{1.4}$$

We now have to calculate $\langle i | [z-E_0(N)+H] | j \rangle$ and to invert the corresponding matrix. To calculate $\langle j | T | \phi \rangle$ we need the ground state $|\phi\rangle$ which is calculated variationally in terms of some basis set $\{|\nu\rangle\}$.

In general, the formulation (1.4) would require a very large basis set to be accurate. Because of the particular form of the Anderson model a "small" set is sufficient if N_f is large. The limit $N_f\to\infty, N_f\Delta=\text{const}$ is of particular interest since the degeneracy, $N_f=14$, of the f level is large. In this limit, we obtain the exact core and valence photoemission spectra as well as the $3d\to 4f$ XAS spectra for the Anderson model. We also find that for finite $N_f\gtrsim 6$ our method gives quite accurate results. This formulation also has other advantages. The spectrum $\mathrm{Im}(\epsilon-i0^+)/\pi$ is non-negative for all energies. The method gives a variational estimate of the threshold, ϵ_{th}, where $\mathrm{Im}g(\epsilon-i0^+)/\pi=0$ for $\epsilon>\epsilon_{\mathrm{th}}$. Even a fairly small basis set can therefore lead to a rather good estimate of ϵ_{th}. Above ϵ_{th} there are of course no unphysical poles. This is in contrast to Green's-function decoupling techniques where it is often hard to find approximations which can avoid unphysical poles for the whole range of parameters. Method (1.4) gives results which are relatively easy to interpret. For instance, we can neglect basis states with a definite physical meaning in the calculation of $|\phi_0\rangle$ (initial-state effects) or in the inversion of the resolvent operator (final-state effects). By studying the effects on the spectrum we can trace the origin of the structures in the spectrum.

While the calculation of the core spectrum requires a matrix inversion, we obtain analytical results for the $3d\to 4f$ XAS and valence[32] photoemission spectra. The valence spectrum $\rho_v(\epsilon)$ is particularly interesting since we obtain a Kondo-type peak at the Fermi energy ϵ_F. For $N_f\gtrsim 6$ the theory fulfils an exact relation between $\rho_v(\epsilon_F)$ and n_f to within 10%. Kondo-type effects in Ce have been discussed earlier by Allen and Martin.[33]

In Sec. II we define the model and perform a transformation which is useful for the later calculations. A simple calculation of the ground state for an infinite f-f Coulomb interaction U is given in Sec. III and it is shown that this calculation becomes exact for $N_f\to\infty$, where N_f is the degeneracy of the f level. A calculation which is more accurate for a finite N_f is presented in Appendix B, where U also is allowed to be finite. Some qualitative aspects of the core-level spectrum are discussed in Sec. IV. In particular it is shown that our method gives the exact core spectrum for $N_F\to\infty$. In Appendix D we give an analytical solution for the case when double occupancy of the f level is neglected, and in Appendix E we show in detail how to calculate the core spectrum when double occupancy is allowed. The calculation of the $3d\to 4f$ XAS spectrum is described in Sec. V. In Sec. VI we show how the valence photoemission spectrum is calculated and discuss some qualitative aspects of the results. In Appendix F we perform a simple calculation of the valence spectrum for a magnetic compound. In Sec. VII the method for performing the BIS calculations is presented. We also consider the combined photoemission and BIS spectra with emphasis on the variation of the number of peaks and their widths when the parameters are varied. In Sec. VIII we discuss the static $T=0$ susceptibility and in Sec. IX the determination of the f occupancy from lattice-parameter data. In Sec. X we apply the theory to $CeNi_2$ and show how n_f and Δ can be deduced from the experimental data. Some aspects of this are also discussed in Sec. IV and VII. Some of these results have been briefly described earlier.[34]

II. MODEL

As discussed in the Introduction, we use the (single-impurity) Anderson model,[19]

$$H=\sum_{k,\sigma}\epsilon_k n_{k\sigma}+[\epsilon_f-U_{fc}(1-n_c)]\sum_{m,\sigma} n_{m\sigma}+\epsilon_c n_c + \sum_{k,m,\sigma}(V_{km}\psi^{\dagger}_{m\sigma}\psi_{k\sigma}+\mathrm{H.c.})+U\sum_{\substack{m,m'\\ \sigma,\sigma'}}{}' n_{m\sigma}n_{m'\sigma'} , \tag{2.1}$$

where ϵ_k describes the conduction states, ϵ_f is the energy of the f level, and ϵ_c describes a core level. The f level has an n-fold orbital degeneracy (m) in addition to the spin degeneracy (σ). In most examples we use $n=7$, which leads to the total degeneracy $N_f=2n=14$. This is appropriate for an f level if spin-orbit splitting is neglected. In Appendix A we discuss the effects of taking the spin-orbit splitting into account. The hopping between the f level and the conduction states is described by V_{km} and the Coulomb interaction between the f electrons is given by U. In addition to the original Anderson model there is a term containing U_{fc} which describes the interaction between a core hole and the f electrons. Multiplet effects are entirely neglected, since U is m independent and there are no exchange integrals. Multiplet effects are observed in the spectroscopies for which there are important final states with mainly f^2 character. For the core spectroscopies there are additional effects due to the multiplet splitting of configurations containing a core hole and one or two f electrons. The Coulomb interaction between the f electrons and the conduction electrons is not explicitly taken into account, but is assumed to be implicitly included as a renormalization of ϵ_f and U.

We shall basically treat the V_{km} as adjustable parameters. For the following derivation, however, we need to

consider the m dependence. Following Bringer and Lustfeld,[35] we assume

$$\sum_k V_{km}^* V_{km'} \delta(\epsilon-\epsilon_k) = \sum_k |V_k|^2 \delta(\epsilon-\epsilon_k)\delta_{mm'} \equiv |V(\epsilon)|^2 \delta_{mm'} . \quad (2.2)$$

This result would, for instance, follow if we assumed that the conduction electrons were in free-electron states. Then

$$V_{km} \sim Y_{3m}(k) ,$$

where $Y_{3m}(k)$ is a spherical harmonic with $l=3$ and the constant-energy surfaces in $\vec{k}$ space are spheres. The assumption (2.2) is, however, *not* limited to free-electron states. It is based on the rapid variation of the phase of V_{km} with k, which means that the k sum in (2.2) is small unless $m=m'$. A more general discussion of Eq. (2.2) was given by Bringer and Lustfeld.[35] The Fermi energy ϵ_F is set equal to zero and the bottom of the band is located at $-B$. We also introduce an upper cutoff B' of the band, although this is not necessary. The coupling Δ can now be defined in terms of $|V(\epsilon)|^2$. One can, for instance, use the maximum value of $\pi|V(\epsilon)|^2$ or an average of $\pi|V(\epsilon)|^2$ over the occupied band. It is useful to introduce new one-particle states,

$$|\epsilon,m\sigma\rangle = V(\epsilon)^{-1} \sum_k V_{km}^* \delta(\epsilon-\epsilon_k)|k,\sigma\rangle . \quad (2.3)$$

States with different m values are orthogonal due to Eq. (2.2). The Hamiltonian can now be rewritten as

$$H = \sum_{\nu=1}^{N_f} \left[\int \epsilon \psi_{\epsilon\nu}^\dagger \psi_{\epsilon\nu} d\epsilon + [\epsilon_f - U_{fc}(1-n_c)]\psi_\nu^\dagger \psi_\nu + \int [V(\epsilon)\psi_\nu^\dagger \psi_{\epsilon\nu} + \text{H.c.}] d\epsilon + U \sum_{\nu<\mu} n_\nu n_\mu \right] + \epsilon_c n_c + \tilde{H}_0 . \quad (2.4)$$

We have introduced a combined index $\nu=(m,\sigma)$ for the orbital and spin degeneracies since these degeneracies are equivalent when the model assumption (2.2) is used. Thus $\epsilon\nu$ refers to a conduction state and ν to a f state. The term $\tilde{H}_0$,

$$\tilde{H}_0 = \sum_\alpha \int \epsilon \psi_{\epsilon\alpha}^\dagger \psi_{\epsilon\alpha} d\epsilon , \quad (2.5)$$

contains the remaining linear combinations of states $|k\sigma\rangle$ orthogonal to the states $|\epsilon,\nu\rangle$ defined in Eq. (2.3). These states, $|\epsilon,\alpha\rangle$, do not couple to the f level and lead to a constant-energy shift which is of no importance. The Hamiltonian (2.4) conserves the number of electrons,

$$\int \psi_{\epsilon\nu}^\dagger \psi_{\epsilon\nu} d\epsilon + \psi_\nu^\dagger \psi_\nu , \quad (2.6)$$

corresponding to a given value of ν.

III. GROUND STATE

We calculate the ground state of (2.4) variationally[3] using Brillouin-Wigner perturbation theory as a guide to which basis states to include. We first introduce a state

$$|0\rangle = \left[\prod_{\nu=1}^{N_f} \prod_{\epsilon\le\epsilon_F} \psi_{\epsilon\nu}^\dagger \right] \left[\prod_\alpha \prod_{\epsilon\le\epsilon_F} \psi_{\epsilon\alpha}^\dagger \right] \psi_c^\dagger |\text{vacuum}\rangle , \quad (3.1)$$

where all the conduction states below the Fermi energy are occupied and the f level is empty. In (3.1) the core level is occupied. The Fermi energy ϵ_F will in the following be set equal to zero. The rest of the states are obtained by repeatedly letting H act on $|0\rangle$. Thus we introduce a set of states

$$|\epsilon\rangle = \frac{1}{\sqrt{N_f}} \sum_\nu \psi_\nu^\dagger \psi_{\epsilon\nu} |0\rangle , \quad (3.2)$$

with one f electron and one hole below ϵ_F. We can form other states, i.e.,

$$\sum_\nu c_\nu \psi_\nu^\dagger \psi_{\epsilon\nu} |0\rangle ,$$

of this type. However, if these states are orthogonal to $|\epsilon\rangle$ ($\sum c_\nu = 0$), they do not couple to $|0\rangle$ via H and they do not enter the ground state calculation. The states (3.2) couple to two sets of states,

$$|E,\epsilon\rangle = \frac{1}{\sqrt{N_f}} \sum_\nu \psi_{E\nu}^\dagger \psi_{\epsilon\nu} |0\rangle , \quad (3.3)$$

with one conduction electron E ($>\epsilon_F$), one hole ϵ, and states

$$|\epsilon,\epsilon'\rangle = \frac{1}{\sqrt{N_f(N_f-1)}} \sum_{\nu,\nu'} \psi_\nu^\dagger \psi_{\epsilon\nu} \psi_{\nu'}^\dagger \psi_{\epsilon'\nu'} |0\rangle \quad (3.4)$$

with two f electrons and two conduction holes. States (3.4) play an important role in the spectroscopies where a core hole is created. Finally we introduce states

$$|E,\epsilon,\epsilon';1\rangle = \frac{1}{\sqrt{N_f}} \sum_\nu \psi_{E\nu}^\dagger \psi_{\epsilon\nu} \psi_{\nu'}^\dagger \psi_{\epsilon'\nu} |0\rangle \quad (3.5)$$

and

$$|E,\epsilon,\epsilon';2\rangle = \frac{1}{\sqrt{N_f(N_f-1)}} \sum_{\substack{\nu,\nu' \\ \nu\neq\nu'}} \psi_{E\nu}^\dagger \psi_{\epsilon\nu} \psi_{\nu'}^\dagger \psi_{\epsilon'\nu'} |0\rangle , \quad (3.6)$$

with one f electron, one conduction electron, and two holes. These states couple to states (3.3), and in addition states (3.6) couple to (3.4). The states (3.4) and (3.5) are limited to $\epsilon>\epsilon'$ as the basis functions otherwise would be linearly dependent. A variational calculation[36] of the ground state using the basis functions $|0\rangle$ and $|\epsilon\rangle$ leads to the same results as first-order Brillouin-Wigner perturbation theory.[31,35] We therefore refer to such a calculation as a first-order treatment. A solution which also includes the states $|E\epsilon\rangle$ is called a second-order calculation, although it also includes terms beyond second-order Brillouin-Wigner perturbation theory. Here we show how the first-order calculation is performed when double occupancy of the f level [states (3.4)] is neglected. In Appendix B we perform a second-order calculation including double occupancy.

For the first-order ground state $|\phi_0^{(1)}\rangle$ we use the ansatz[36]

$$|\phi_0^{(1)}\rangle = A\left[|0\rangle + \int_{-B}^{0} a(\epsilon)|\epsilon\rangle d\epsilon\right], \tag{3.7}$$

where the integral over ϵ is limited to the states below $\epsilon_F = 0$. We define

$$\Delta E = E_0^{(1)}(N) - \langle 0|H|0\rangle \equiv E_0^{(1)}(N) - E_0^0, \tag{3.8}$$

where $E_0^{(1)}(N)$ is the ground-state energy. Thus ΔE is the lowering of the energy when the impurity is introduced. Minimization of ΔE gives the secular equations

$$\Delta E = \sqrt{N_f}\int [V(\epsilon)]^* a(\epsilon) d\epsilon, \tag{3.9}$$

$$(\Delta E - \epsilon_f + \epsilon) a(\epsilon) = \sqrt{N_f} V(\epsilon), \tag{3.10}$$

where we have used

$$\langle \epsilon|H|0\rangle = \sqrt{N_f} V(\epsilon). \tag{3.11}$$

Solving (3.9) and (3.10) we obtain[36,31]

$$\Delta E = N_f \int \frac{|V(\epsilon)|^2}{\Delta E - \epsilon_f + \epsilon} d\epsilon, \tag{3.12}$$

$$n_f \equiv A^2 \int |a(\epsilon)|^2 d\epsilon = \frac{C}{1+C}, \tag{3.13}$$

where

$$C = N_f \int \frac{|V(\epsilon)|^2}{(\Delta E - \epsilon_f + \epsilon)^2} d\epsilon \tag{3.14}$$

and

$$A = (1+C)^{-1/2} = \sqrt{1-n_f}. \tag{3.15}$$

If $V(\epsilon) \equiv V$ is a constant within the band and $|\Delta E - \epsilon_f| \ll B$, we obtain

$$\Delta E \approx N_f V^2 \ln\left|\frac{\Delta E - \epsilon_f}{B}\right|, \tag{3.16}$$

$$C \approx N_f V^2 \frac{1}{|\Delta E - \epsilon_f|}. \tag{3.17}$$

Due to the variational nature of the calculation $\Delta E < \epsilon_f$. In the spin-fluctuation limit $n_f \approx 1$, the formulas can be further simplified, as described in Appendix C.

In the model (2.1) the degeneracy N_f of the f level is 14. If spin-orbit splitting is taken into account and only the lower of the two spin-orbit-split levels is considered we obtain $N_f = 6$. In both cases N_f is large and it is interesting to study the limit $N_f \to \infty$. Since N_f enters Eqs. (3.12)–(3.17) in the combination $N_f |V(\epsilon)|^2$ it is useful to consider the limit

$$N_f \to \infty, \quad N_f |V(\epsilon)|^2 = \text{const}, \tag{3.18}$$

since in this limit the first-order solution stays constant and the exact solution converges. We now apply the Hamiltonian to the first-order ground state (3.7) assuming that double occupancy is suppressed ($U = \infty$). This leads to

$$H|\phi_0^{(1)}\rangle = E_0^{(1)}(N)|\phi_0^{(1)}\rangle + A\int_0^{B'}\left[\int_{-B}^{0}[V(E)]^* a(\epsilon)|E,\epsilon\rangle d\epsilon\right] dE, \tag{3.19}$$

where the E integral is limited to the states above $\epsilon_F = 0$. Since $|\phi_0^{(1)}\rangle$ was obtained by diagonalizing H in a subspace of all possible states, we recover this state. However, H can also connect the states $|\epsilon\rangle$ to the states $|E,e\rangle$ outside the subspace and we obtain the second term in Eq. (3.19). The norm of this term is

$$A^2 \int_0^{B'}\left[\int_{-B}^{0}|V(E)|^2 |a(\epsilon)|^2 d\epsilon\right] dE \le \int_0^{B'} |V(E)|^2 dE. \tag{3.20}$$

Thus in the limit (3.18) the norm of the second state in (3.19) goes to zero and the state (3.7) is the exact ground state.[34,37] The total space of states splits up in disconnected subspaces in the limit (3.18). We have

$$\langle E,\epsilon|H|\epsilon\rangle = [V(E)]^*, \tag{3.21}$$

which goes to zero for $N_f \to \infty$, while the matrix element between $|0\rangle$ and $|\epsilon\rangle$ [Eq. (3.11)] remains finite. Thus $|0\rangle$ and $|\epsilon\rangle$ form a subspace which does not couple to any other state in this limit. This is related to the observation that there are N_f ways of going from $|0\rangle$ to a state $\psi_\nu^\dagger \psi_{\epsilon\nu}|0\rangle$ ($1 \le \nu \le N_f$), while there is only one way of going from $\psi_\nu^\dagger \psi_{\epsilon\nu}|0\rangle$ to $\psi_{E\nu}^\dagger \psi_{\epsilon\nu}|0\rangle$. Similarly, the states $|E,\epsilon\rangle$, $|E,\epsilon,\epsilon';1\rangle$, and $|E,\epsilon,\epsilon';2\rangle$ form a subspace without coupling to other states in the limit $N_f \to \infty$ (if double occupancy is neglected).

For finite N_f all these higher states contribute to the exact ΔE. However, each time we take a higher subspace of the types (3.3) and (3.6) into account, the corresponding contribution is one order higher in $1/N_f$. Thus for $N_f |V(\epsilon)|^2$ fixed states (3.3) and (3.6) give a contribution of the order N_f^{-1}. As pointed out before we define the order of the calculation in terms of the basis states. Thus a first-order calculation includes the states (3.1), (3.2), and (3.4) if double occupancy is not suppressed. A second-order calculation also includes state (3.4) and a third-order calculation the states (3.5) and (3.6). The first- and second-order calculations lead to errors in ΔE of the order $1/N_f$, while the errors in the third-order calculation are of the order $1/N_f^2$ for $U = \infty$. If the states (3.5) are neglected in the third-order calculation, the errors remain of the order $1/N_f^2$, but the calculation is simplified substantially. If double occupancy cannot be neglected some additional states have to be included to avoid errors of the order $1/N_f$.

To test the accuracy of the ground-state calculation we have first applied the theory to a nondegenerate system ($N_f = 1$) where we can obtain the exact result. For $|V(\epsilon)|^2$ we have used a semielliptical form symmetric around $\epsilon_F = 0$,

$$\pi |V(\epsilon)|^2 = 2V^2(B^2 - \epsilon^2)^{1/2}/B^2. \tag{3.22}$$

We define

$$\Delta = \pi \max_\epsilon[|V(\epsilon)|^2] = 2V^2/B.$$

In Fig. 2 we show results for ΔE [Eq. (3.8)] as a function of ϵ_f. The figure shows the first-order result (3.12), the second-order result obtained by using the states (3.1)–(3.3), and the third-order result based on the states (3.1)–(3.3), (3.5) and (3.6). Since the expansion parameter $1/N_f = 1$ is not small, we do not expect the first-order result to be particularly accurate, except for $\epsilon_f \gg \Delta$, where

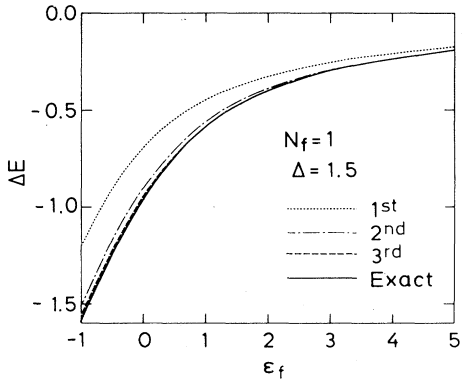

FIG. 2. Energy ΔE [Eq. (3.8)] as a function of ϵ_f for a nondegenerate system. The density of states was given by Eq. (3.22) with $B=3$ eV and $\Delta=1.5$ eV. First-, second-, and third-order calculations are compared with the exact result.

Δ/ϵ_f provides a small parameter. The figure shows, however, that the second-order result is fairly accurate over the whole range. The lower limit, $\epsilon_f=-1$, corresponds to an occupancy $n_f=0.74$. In Fig. 3 we show ΔE and n_f as a function of N_f for a fixed value of $N_f\Delta$. The figure illustrates how the first-order theory becomes increasingly accurate as N_f is increased. For $N_f=14$ the difference in ΔE between the first- and third-order calculations is 0.03, and the difference in n_f between the first- and second-order calculations is 0.007.

IV. XPS CORE SPECTRUM

In the sudden approximation the core-level photoemission current is directly related to the core spectrum

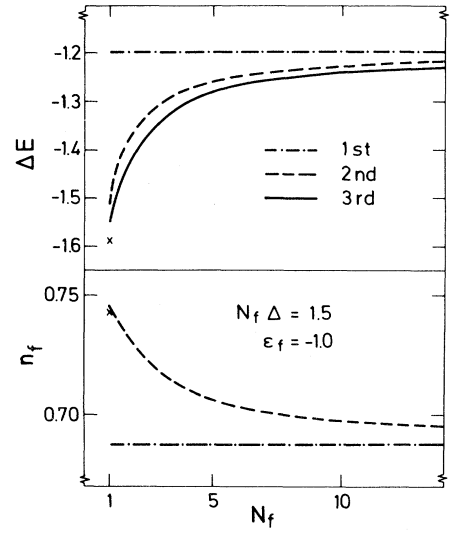

FIG. 3. Energy ΔE [Eq. (3.8)] and the f occupancy n_f for a semielliptical density of states [Eq. (3.22)] as a function of the degeneracy N_f for a fixed value of $N_f\Delta=1.5$ eV. Figure shows results of the first- (dashed-dotted curve), second- (dashed curve), and third- (solid curve) order calculations. For $N_f=1$ the crosses show the exact results. Parameters are $\epsilon_f=-1$ eV and $B=3$ eV. Observe the vertical scale.

$$j(\epsilon)\sim\rho_c(\epsilon-\hbar\omega)\equiv\frac{1}{\pi}\,\mathrm{Im}g_c(z-\hbar\omega)\ , \tag{4.1}$$

where

$$g_c(z)=\langle\phi_0\,|\,\psi_c^\dagger\frac{1}{z-E_0(N)+H}\psi_c\,|\,\phi_0\rangle \tag{4.2}$$

and $z=\epsilon-iy$. In the theoretical discussion y is an infinitesimal positive quantity, while it is finite in the numerical work, to simplify the calculation and to describe Lorentzian life-time broadening. As indicated in the Introduction, we introduce a basis set $\{\,|\,i\,\rangle\}$, consisting of some of the states (3.1)—(3.6) with the core level empty. We can then obtain an approximate expression for $g_c(z)$ by assuming that these basis states form a complete set of states[34]

$$g_c(z)=\sum_{i,j}\langle\phi_0\,|\,\psi_c^\dagger\,|\,i\,\rangle\left\langle i\left|\frac{1}{z-E_0(N)+H}\right|j\right\rangle\langle j\,|\,\psi_c\,|\,\phi_0\rangle\ , \tag{4.3}$$

and invert the matrix $\langle i\,|\,[z-E_0(N)+H]\,|\,j\,\rangle$. Because of the operators ψ_c and $\psi_c^\dagger$ in (4.2), the final-state Hamiltonian $H(n_c=0)$ enters the problem where we set $n_c=0$ in Eq. (2.1). An important property of this approach becomes obvious if we transform to new states $|\,n\,\rangle$, which diagonalize $H(n_c=0)$ in the space $\{\,|\,i\,\rangle\}$. Our approximate core spectrum can then be written as

$$\rho_c(\epsilon)=\sum_n|\,\langle\epsilon_n(N-1)\,|\,\psi_c\,|\,\Phi_0\rangle\,|^2\times\delta(\epsilon-\epsilon_0(N)+\epsilon_n(N-1))\ . \tag{4.4}$$

This expression differs from the exact one [Eq. (1.1)] by the appearance of approximate states, $|\,\Phi_0\rangle$ and $|\,\epsilon_n(N-1)\rangle$, and energies, $\epsilon_0(N)$ and $\epsilon_n(N-1)$, due to the use of a finite basis set.

It is now obvious that (4.4) is positive for all energies independently of the quality of the basis set. Furthermore, (4.4) is zero above the threshold

$$\epsilon_{\mathrm{th}}=\epsilon_0(N)-\epsilon_0(N-1)\ . \tag{4.5}$$

The error in ϵ_{th} depends on the completeness of the basis set and the degree of cancellation of errors in $\epsilon_0(N)-\epsilon_0(N-1)$. Owing to the variational principle the description of the threshold should put moderate demands on the basis set. For the same reason one may expect that the positions of the peaks in the spectrum are reasonably well reproduced and that the appearance of unphysical peaks is unlikely. This is in contrast to Green's-function decoupling techniques where it often is hard to suppress unphysical poles over the whole parameter range. This formulation is convenient to use for a discussion of the limit (3.18) ($N_f\to\infty$). We showed in Sec. III that our method leads to the correct ground state $|\,\phi_0\rangle$ in this limit.[37] Since the exact expression for the spectral density and expression (4.4) are identical in form, the proof that (4.4) is exact for $N_f\to\infty$ just requires that we show that $|\,\epsilon_n(N-1)\rangle$ and $\epsilon_n(N-1)$ are exact eigenstates and eigenenergies, respectively. It is *not* necessary to find *all* the eigenstates. To calculate (1.1) we only need the ones

which exhaust the sum rule

$$\sum_n |\langle \epsilon_n(N-1)|\psi_c|\phi_0\rangle|^2=1 , \tag{4.6}$$

since the remaining ones do not contribute to the sum in Eq. (1.1). In the following we indicate the proof for the case when double occupancy of the f level is allowed but higher occupancies are suppressed. We proceed as in Sec. III and diagonalize $H(n_c=0)$ in the space of the state equivalent to (3.1), (3.2), and (3.4), but with the core level empty. This leads to

$$|\epsilon_n(N-1)\rangle=A_n\left[|\tilde{0}\rangle+\int_{-B}^{0}d\epsilon a_n(\epsilon)|\tilde{\epsilon}\rangle+\int_{-B}^{0}d\epsilon\left[\int_{-B}^{\epsilon}d\epsilon' c_n(\epsilon,\epsilon')|\tilde{\epsilon},\tilde{\epsilon}'\rangle\right]\right] , \tag{4.7}$$

where

$$|\tilde{0}\rangle=\psi_c|0\rangle \tag{4.8}$$

and $|\tilde{\epsilon}\rangle$ and $|\tilde{\epsilon},\tilde{\epsilon}'\rangle$ are states with a core hole. In the following we suppress the tilde. We now apply H to $|\epsilon_n(N-1)\rangle$,

$$H|\epsilon_n(N-1)\rangle=\epsilon_n(N-1)|\epsilon_n(N-1)\rangle +A\int_0^{B'}dE\left[[V(E)]^*\left[\int_{-B}^{0}d\epsilon a_n(\epsilon)|E,\epsilon\rangle+\int_{-B}^{0}d\epsilon\int_{-B}^{\epsilon}d\epsilon' c_n(\epsilon,\epsilon')(|E,\epsilon,\epsilon';2\rangle+|E,\epsilon',\epsilon;2\rangle)\right]\right] . \tag{4.9}$$

Since the second term in (4.9) contains $V(E)$ without a factor $\sqrt{N_f}$, we can show as in Sec. III that the norm of the additional state goes to zero for $N_f\to\infty$. The states $|\epsilon_n(N-1)\rangle$ are therefore exact eigenstates.[37] Since they are obtained in the same valence electron subspace as $|\phi_0\rangle$ they exhaust the sum rule (4.6) and this approach therefore yields the exact spectrum in the limit (3.18), assuming that more than double occupancy of the f level can be neglected.[34,37]

In Appendix D we obtain the analytic first-order spectrum for the case when double occupancy is suppressed. This solution is of interest for La compounds. In Appendix E we derive formulas for a second-order calculation of the core spectrum when double occupancy is allowed.

Figure 4 shows the core spectrum for a nondegenerate system. The first-order solution gives peaks at about the right energy but the weights are off by about a factor of 2. This is consistent with the variational arguments below Eq. (4.5) that even a rather poor basis set can give good peak positions. Already the second-order solution, however also gives the weights of the peaks in fairly good agreement with the exact solution.[27] Figure 5 shows results for $N_f=6$. In this case the difference between the first- and second-order calculations is very small, indicating that already for $N_f=6$ the first-order solution is fairly accurate. The figure also shows a calculation where double occupancy has been suppressed in the initial state. Although the double occupancy ($|c_2|^2$) in the initial state for realistic values of U and Δ is quite small (<0.05), it strongly influences the f^2 peak of the XPS core spectrum. To understand this effect we consider the model in Fig. 1. The fi-

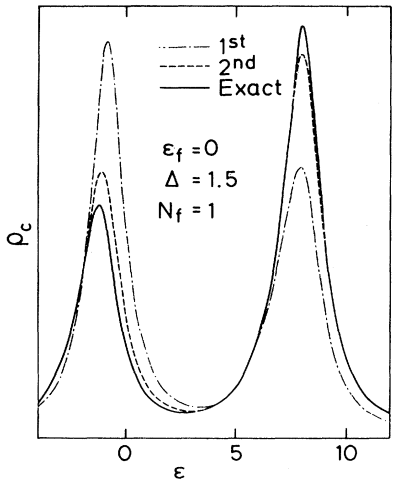

FIG. 4. Core-level spectrum in the nondegenerate ($N_f=1$) case. First- (dashed-dotted curve) and second- (dashed curve) order treatments are compared with the exact spectrum. We have used a semielliptical symmetric density of states [(3.22)], with $\epsilon_f=0$, $\Delta=1.5$, $B=3$, and $U_{fc}=9$. All energies are given in eV. A Lorentzian broadening of 1.8 eV (FWHM) was used.

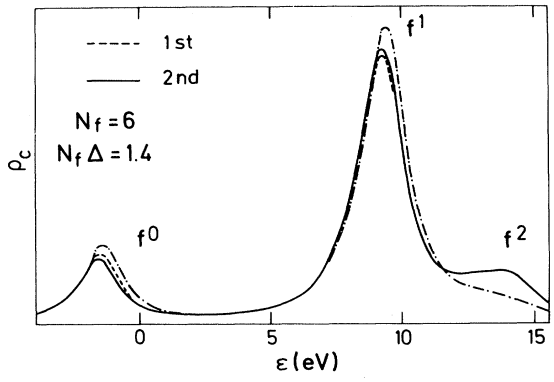

FIG. 5. Core-level spectrum for $N_f=6$. First- (dashed curve) and second- (solid curve) order treatments are compared with a second-order calculation (dashed-dotted curve) where double occupancy is suppressed in the initial state. We have used the parameters $\epsilon_f=-1.1$, $U_{fc}=10$, $U=6$, $B=3$, and $N_f\Delta=1.4$ eV. For these parameters the double occupancy is 0.02. Peaks are labeled according to the number of f electrons in the corresponding final states. A Lorentzian broadening of 1.8 eV (FWHM) was used.

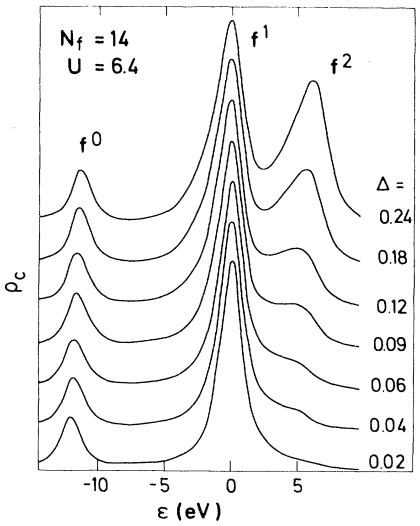

FIG. 6. Core-level x-ray photoemission spectrum as a function of the coupling Δ between the f level and the conduction states. Spectra are normalized to the height of the f^1 peak and the f^1 peaks are lined up. A Lorentzian broadening of 1.8 eV (FWHM) was introduced. Conduction band was described by Eq. (4.10) with the parameters $\epsilon_0=-1.22$, $B=2.79$, $U=6.4$, and $\epsilon_f-U_{fc}=-11.8$, where all energies are in eV. f^0 weight of the initial state was kept at 0.2.

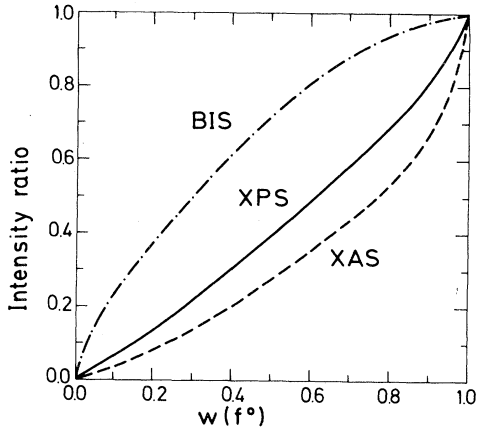

FIG. 7. Intensity ratio $I(f^1)/[I(f^1)+I(f^2)]$ for the XAS (dashed curve) and the BIS (dashed-dotted curve) spectra and $I(f^0)/[I(f^0)+I(f^1)+I(f^2)]$ for the XPS (solid curve) spectrum as a function of the f^0 weight $w(f^0)$ in the initial state. Parameters are $\Delta=0.12$, $N_f=14$, $\epsilon_0=-1.22$, and $B=2.79$ [Eq. (4.10)]. We used $U=6.4$ and $\epsilon_f-U_{fc}=11.9$ for the XPS and XAS spectra and $\epsilon_f+U=4$ for the BIS spectrum, with all energies in eV.

nal state corresponding to the f^2 peak is approximately $|\tilde{f}^2\rangle=c_1^1|f^1\rangle+c_2^1|f^2\rangle$. According to Eq. (1.1), the weight of the f^2 peak is $p=|c_1c_1^1+c_2c_2^1|^2$. Since both c_1^1 and c_2 are small, the relative change of p is large if we set $c_2=0$. Figure 6 shows the core spectrum as function of Δ. Following an earlier publication,[21] we have used

$$\pi|V(\epsilon)|^2=2V^2[B^2-(\epsilon-\epsilon_0)^2]^{1/2}/B^2\ , \tag{4.10}$$

where $\epsilon_0=-1.22$ eV and $B=2.79$ eV, which may be used to describe Ce compounds with transition elements. The weight of the f^2 peak depends strongly on Δ, and this weight can therefore be used to estimate Δ for Ce compounds. In Fig. 7 we show the weight of the f^0 peak as a function of the probability, $w(f^0)\approx 1-n_f$, of having no f electron in the initial state. This figure will be discussed in detail in Sec. VII. However, we note that even for a fairly large value of Δ, the difference between $w(f^0)$ and the weight of the f^0 peak is not very large. The XPS spectrum therefore provides information about both Δ and n_f, and in another paper we have presented estimates of these parameters for a large number of La and Ce compounds.[21]

V. X-RAY-ABSORPTION SPECTROSCOPY

XAS has been used to study the f occupancy.[14,15] Normally the $L_{\rm III}$ edge is studied, which primarily involves a $2p\rightarrow 5d$ transition. Our present Hamiltonian (2.1) is less suited to study this transition since it does not explicitly take into account the Coulomb interaction between the d electrons, on the one hand, and the core hole and f electrons, on the other. Recently, there have also been experiments for the $3d\rightarrow 4f$ transition.[20] The Hamiltonian (2.1) is more appropriate for this process and below we present a theoretical description.

We introduce the operator

$$T=\sum_\nu W_\nu\psi_\nu^\dagger\psi_c \tag{5.1}$$

to describe the excitation $3d\rightarrow 4f$. In the limit (3.18) it is convenient to consider $\sum_\nu|W_\nu|^2\rightarrow$const since the XAS spectrum then converges. The x-ray-absorption spectrum is given by

$$I(\omega)\sim\frac{1}{\pi}\mathrm{Im}\left\langle\phi\left|T^\dagger\frac{1}{z+E_0(N)-H}T\right|\phi\right\rangle\ , \tag{5.2}$$

where $z=\omega-iy$. The photon energy is ω and we have as usual introduced a life-time broadening $2y$. We develop a theory which is correct[37] in the limit (3.18) ($N_f\rightarrow\infty$). Double occupancy in the initial state is taken into account and $|\phi_0\rangle$ is therefore given by (B1), except for the second-order term $|E\epsilon\rangle$, which is neglected. We introduce states

$$|\nu\rangle=\psi_\nu^\dagger|0\rangle\ , \tag{5.3}$$

$$|\epsilon\nu\rangle=\frac{1}{\sqrt{N_f-1}}\sum_{\nu'\neq\nu}\psi_\nu^\dagger\psi_{\nu'}^\dagger\psi_{\epsilon\nu'}|0\rangle\ , \tag{5.4}$$

where $|0\rangle$ now means a state with a core hole since the $\sim$ in Eq. (4.8) is suppressed. These are the only states which couple to the first-order ground state apart from states with three f electrons, which are neglected here. As in Sec. IV we can also show that these are the states needed to obtain the correct result for $N_f\rightarrow\infty$.[37] We can now calculate the matrix elements of $(z+E_0(N)-H)^{-1}$ between $|\nu\rangle$ and $|\nu'\rangle$ using the fact that the Hamiltonian (2.4) conserves the number of "ν" electrons [Eq. (2.6)]. We obtain

$$\left\langle \nu \left| \frac{1}{z+E_0(N)-H} \right| \nu' \right\rangle = g_{\mathrm{XAS}}(z)\delta_{\nu\nu'} = \frac{\delta_{\nu\nu'}}{z+\Delta E+\epsilon_c-\epsilon_f+U_{fc}+(N_f-1)\tilde{\Gamma}(-z-\Delta E-\epsilon_c+2\epsilon_f-2U_{fc}+U)} , \quad (5.5)$$

where $\tilde{\Gamma}$ is defined in Eq. (D7). The minus sign enters because the resolvent operator in this case contains $-H$. We can now express the other matrix elements of $[z+E_0(N)-H]^{-1}$ in terms of $g_{\mathrm{XAS}}(z)$ using the same technique as for the core spectrum (Appendix E). We define

$$h(z)=\frac{1}{\sqrt{N_f}} \int_{-B}^{0} d\epsilon \frac{a(\epsilon)[V(\epsilon)]^*}{z+\Delta E+\epsilon_c-2\epsilon_f+2U_{fc}-U+\epsilon} , \quad (5.6)$$

and obtain the spectrum

$$I(z)=\frac{1}{\pi}A^2 \sum_{\nu} |W_\nu|^2 \mathrm{Im} \left[g_{\mathrm{XAS}}(z)[1+(N_f-1)h(z)]^2+(N_f-1)\int_{-B}^{0} \frac{|a(\epsilon)|^2/N_f}{z+\Delta E+\epsilon_c-2\epsilon_f+2U_{fc}-U+\epsilon} d\epsilon \right] . \quad (5.7)$$

In Fig. 8 we show some typical XAS spectra for different values of n_f. The spectra show two peaks corresponding to f^1 and f^2 final states. To be able to compare the XAS and XPS spectra, we arrange the energy axis in both cases so that the peak corresponding to the lowest final state is to the right. Since in the $3d \rightarrow 4f$ XAS process an f electron is added to the valence system, we expect the weight of the f^1 peak to vary with $w(f^0)$, the weight of the f^0 configuration in the initial state. The figure shows that there is such a relation, but that the weight of the f^1 peak is substantially smaller than $w(f^0)$. This is illustrated more quantitatively in Fig. 7 which is discussed in Sec VII.

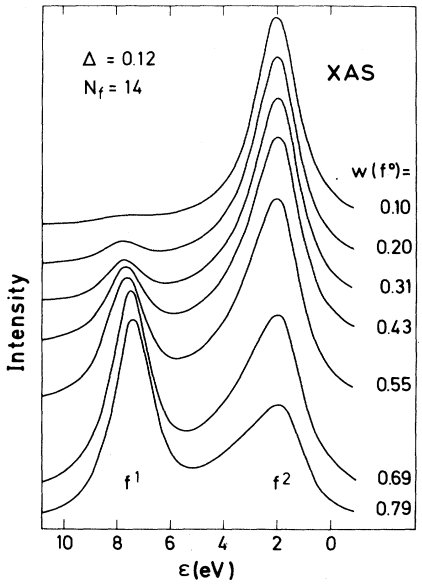

FIG. 8. $3d \rightarrow 4f$ XAS spectrum as a function of the f^0 weight $w(f^0)$ in the ground state. Spectra are normalized to the height of the larger peak and the f^2 peaks are lined up. We have used the parameters [Eq. (4.10)] $\epsilon_0=-1.22$, $B=2.79$, $V=0.41$, $U=6.4$, and $\epsilon_f-U_{fc}=-11.9$. Lorentzian broadening of 1.8 eV (FWHM) has been introduced and all energies are in eV.

VI. VALENCE PHOTOEMISSION

Photoemission from the valence band has often been used to study the position and width of the f level in Ce compounds.[10–13] We therefore focus on the emission from the f level and describe the photoemission process by

$$T=\sum_{\nu} \tilde{W}_\nu \psi^\dagger_{\tilde{E}\nu}\psi_\nu , \quad (6.1)$$

where $\tilde{E}$ is the energy of a scattering state. In the sudden approximation the photoemission current is given by

$$j(\tilde{E}) \sim -\frac{1}{\pi}\mathrm{Im}\sum_{\nu}\left\langle \phi_0 \left| T^\dagger \psi^\dagger_{\tilde{E}\nu} \frac{1}{\tilde{E}-i0^+-E_0(N)-\omega+H} \psi_{\tilde{E}\nu} T \right| \phi_0 \right\rangle . \quad (6.2)$$

Thus we need to calculate the Green's function

$$g^<(z)=\left\langle \phi_0 \left| \psi^\dagger_\nu \frac{1}{z-E_0(N)+H} \psi_\nu \right| \phi_0 \right\rangle . \quad (6.3)$$

Since the ground state is nonmagnetic, $g^<(z)$ is independent of ν. We show explicitly a calculation correct to lowest order in $1/N_f$. We use the first-order ground state (3.7) and obtain

$$\psi_\nu |\phi_0^{(1)}\rangle = \frac{A}{\sqrt{N_f}} \int d\epsilon\, a(\epsilon)\psi_{\epsilon\nu}|0\rangle . \quad (6.4)$$

We introduce the final-state basis function

$$|\epsilon,\nu\rangle = \psi_{\epsilon\nu}|0\rangle . \quad (6.5)$$

This function couples to

$$|\epsilon,\epsilon',\nu;1\rangle = \frac{1}{\sqrt{N_f-1}} \sum_{\nu'\neq\nu} \psi^\dagger_{\nu'}\psi_{\epsilon'\nu}\psi_{\epsilon\nu}|0\rangle \quad (6.6)$$

and

$$|\epsilon,\epsilon',\nu;2\rangle = \psi^\dagger_\nu\psi_{\epsilon'\nu}\psi_{\epsilon\nu}|0\rangle . \quad (6.7)$$

To avoid overcompleteness in the subspace considered, (6.7) is limited to $\epsilon > \epsilon'$. We need the matrix elements

$$\langle \epsilon,\epsilon',\nu;1|H|\epsilon'',\nu\rangle = \sqrt{N_f-1}V(\epsilon')\delta(\epsilon-\epsilon'') , \quad (6.8)$$

$$\langle \epsilon,\epsilon'\nu;2 \mid H \mid \epsilon'',\nu\rangle = V(\epsilon')\delta(\epsilon-\epsilon'') - V(\epsilon)\delta(\epsilon'-\epsilon'') \ . \tag{6.9}$$

Using arguments of the types (3.19), (3.20), and (4.6), one can see that for $U=\infty$ it is sufficient to use the basis states (6.5) and (6.6) to obtain the exact spectrum in the limit (3.18), $N_f \to \infty$.[37] This follows since both the state $\mid \epsilon,\epsilon',\nu;2\rangle$ and states of the type $\psi^\dagger_{E\nu}\psi_{\epsilon'\nu}\psi_{\epsilon\nu}\mid 0\rangle$ couple to the states (6.5) and (6.6) with the strength V, which goes to zero in the limit $N_f \to \infty$. To calculate the Green's function (6.3) we have to invert $\tilde{H}=z-E_0(N)+H$ in the subspace specified above. Using the basis functions (6.5) and (6.6) we obtain the matrix elements

$$\tilde{H}(\epsilon,\epsilon') = (z-\Delta E-\epsilon)\delta(\epsilon-\epsilon') \ , \tag{6.10}$$

$$\tilde{H}(\epsilon\epsilon',\epsilon_1\epsilon_2) = (z-\Delta E-\epsilon-\epsilon'+\epsilon_f)\delta(\epsilon-\epsilon_1)\delta(\epsilon'-\epsilon_2) \ , \tag{6.11}$$

$$\tilde{H}(\epsilon\epsilon',\epsilon'') = \sqrt{N_f-1}\,V(\epsilon')\delta(\epsilon-\epsilon'') \ , \tag{6.12}$$

with obvious notation. Since (6.11) is diagonal it is convenient to use Eq. (D5), which yields

$$\langle \epsilon,\nu \mid [z-E_0(N)+H]^{-1} \mid \epsilon',\nu\rangle = g(z-\Delta E+\epsilon_f-\epsilon)\delta(\epsilon-\epsilon') \ , \tag{6.13}$$

where

$$g(z) = \frac{1}{z-\epsilon_f-N_f\tilde{\Gamma}(z)} \tag{6.14}$$

and

$$\tilde{\Gamma}(z) = \int_{-B}^{0} \frac{\mid V(\epsilon)\mid^2}{z-\epsilon} d\epsilon \ . \tag{6.15}$$

In (6.14) we have anticipated the more accurate result (6.19) below and used the prefactor N_f in front of $\tilde{\Gamma}(z)$ instead of the factor (N_f-1) which would result from Eqs. (6.11), (6.12), and (D5). The additional term $\tilde{\Gamma}(z)$, which is of the order $1/N_f$, is due to the basis functions (6.7). Equation (6.13) provides the only part of $\tilde{H}^{-1}$ we need, since the basis function $\mid \epsilon,\epsilon',\nu;1\rangle$ do not couple to $\psi_\nu \mid \phi_0^{(1)}\rangle$ [Eq. (6.4)]. Thus we obtain

$$g^<(z) = \frac{A^2}{N_f} \int d\epsilon \mid a(\epsilon)\mid^2 g(z-\Delta E+\epsilon_f-\epsilon) \ . \tag{6.16}$$

For finite N_f we can find a more accurate solution by keeping the basis functions (6.7) and introducing the functions

$$\mid E,\epsilon,\epsilon',\nu;1\rangle = \frac{1}{\sqrt{N_f-1}} \sum_{\nu'\neq\nu} \psi^\dagger_{E\nu'}\psi_{\epsilon'\nu'}\psi_{\epsilon\nu}\mid 0\rangle \ , \tag{6.17}$$

$$\mid E,\epsilon,\epsilon',\nu;2\rangle = \psi^\dagger_{E\nu}\psi_{\epsilon'\nu}\psi_{\epsilon\nu}\mid 0\rangle \ . \tag{6.18}$$

Then we have to invert the matrix

$$[G^<(\epsilon,\epsilon')]^{-1} = [z-\Delta E-\epsilon-N_f\tilde{\Gamma}_2(z-\Delta E+\epsilon_f-\epsilon)]\delta(\epsilon-\epsilon') + \frac{V(\epsilon)V(\epsilon')}{z-\Delta E+\epsilon_f-\epsilon-\epsilon'-\gamma(z-\Delta E-\epsilon-\epsilon')} \ , \tag{6.19}$$

where

$$\tilde{\Gamma}_2(z) = \int_{-B}^{0} \frac{\mid V(\epsilon)\mid^2}{z-\epsilon-\gamma(z-\epsilon_f-\epsilon)} d\epsilon \ , \tag{6.20}$$

and $\gamma(z)$ is defined in Eq. (E7). The Green's function (6.3) is then given by

$$g^<(z) = \frac{A^2}{N_f} \int d\epsilon \int d\epsilon' a(\epsilon)^* G^<(\epsilon,\epsilon') a(\epsilon') \ , \tag{6.21}$$

where $a(\epsilon)$ now should be obtained from a second-order ground-state calculation including states (3.3).

We discuss in more detail the structure of the lowest-order result (6.14)–(6.16). We first observe that $\mathrm{Im}g(\epsilon-i0^+)$ is nonzero for $-B<\epsilon<0$. In addition $g(\epsilon)$ has a pole at $\epsilon=\epsilon_f-\Delta E$. This can be seen from the fact that

$$N_f\tilde{\Gamma}(\epsilon_f-\Delta E) = -\Delta E \ ,$$

which follows from (3.12). The strength of this pole is

$$\left[1-\left[\frac{\partial}{\partial z}N_f\tilde{\Gamma}(z)\right]_{z=\epsilon_f-\Delta E}\right]^{-1} = 1-n_f \ , \tag{6.22}$$

which follows from Eqs. (3.14) and (3.15). Inserting this result into Eq. (6.16) yields

$$\rho_v(\epsilon) \equiv \frac{1}{\pi}\mathrm{Im}N_f g^<(\epsilon-i0^+) = \frac{(1-n_f)^2 N_f \mid V(\epsilon)\mid^2}{(\epsilon+\Delta E-\epsilon_f)^2}, \quad \Delta E-\epsilon_f \le \epsilon \le 0 \tag{6.23}$$

where we have used (3.10) and (3.15). For $\epsilon<\Delta E-\epsilon_f$ the continuum of $\mathrm{Im}g(z)$ also contributes to $\mathrm{Im}g^<(z)$.

Equation (6.23) describes a sharp rise in the spectrum close to ϵ_F. The origin of this structure is the function $N_f\tilde{\Gamma}(z)$ in Eq. (6.14), which results from the interaction between states (6.5) and (6.6). Out of these basis functions we can form linear combinations of the type $\psi_{\epsilon\nu}\mid\phi_0\rangle$, which are identical to the ground state except for a conduction hole at ϵ. These states contribute weight at the energy ϵ, and they have a finite overlap, $(1-n_f)a(\epsilon)/\sqrt{N_f}$, to $\psi_\nu\mid\phi_0\rangle$ [Eq. (6.4)]. It is instructive to compare (6.23) which is exact for $N_f=\infty$ with the exact result for a nondegenerate model, $N_f=1$. In the latter case the imaginary part of the Green's function $g^<(z)$ can be calculated from an expression similar to $g(z)$ defined in (6.14)

$$\rho_v^{N_f=1}(\epsilon) \equiv \frac{1}{\pi}\mathrm{Im}g^<_{N_f=1}(\epsilon-i0^+) = \frac{1}{\pi}\mathrm{Im}\left[\frac{1}{\epsilon-i0^+-\epsilon_f-\Gamma(\epsilon_f-i0^+)}\right]\Theta(-\epsilon) \tag{6.24}$$

where $\Theta(x)$ is the unit step function, and

$$\Gamma(z) = \int_{-B}^{B'} \frac{\mid V(\epsilon)\mid^2}{z-\epsilon} d\epsilon \tag{6.25}$$

now involves an integral over *all* energies in the band, while the integral in (6.15) defining $\tilde{\Gamma}(z)$ is limited to ener-

gies below the Fermi energy $\epsilon_F=0$. The other important difference to the exact result for $N_f=\infty$ is that *no* energy integration as in (6.16) occurs in (6.24). For the comparison of these exact results for $N_f=1$ and $N_f=\infty$ we have to distinguish the cases $\epsilon_f>\epsilon_F$ and $\epsilon_f<\epsilon_F$. For simplicity we assume a broad band ($B\gg N_f\Delta$) with $V(\epsilon)=$const ($\Delta=\pi V^2$). Then the spectral function (6.24) for $N_f=1$ is a Lorentzian of half-width Δ centered at ϵ_f which is cut off above the Fermi energy $\epsilon_F=0$. For $\epsilon_f>\epsilon_F$ the spectral density (6.24) therefore is *rising* with energy as one approaches the Fermi energy from below. This rise is just the onset of the "affinity peak" which lies above ϵ_F. For $\epsilon_f\gg\Delta$ the results for $N_f=1$ [(6.24)] and $N_f=\infty$ [(6.16)] agree to leading order in V^2. This is no surprise as in this case perturbation theory in V works independently of the value of N_f. When ϵ_f lies below the Fermi energy, the $N_f=1$ result leads to an "ionization" peak at ϵ_f and the spectral density at ϵ_F is *decreasing*. This is in strong contrast to the $N_f=\infty$ result [(6.23)] which always shows an *increase* in spectral weight when the Fermi energy is approached from below. If we would extrapolate the $N_f=\infty$ expression [(6.23)] to energies above ϵ_F, $\rho_v(\epsilon)$ would diverge at $\epsilon=\epsilon_f-\Delta E$. [We will see in the following section that the BIS spectral function, which presents the "natural" continuation of $\rho_v(\epsilon)$ above ϵ_F actually has a peak at $\epsilon_F-\Delta E$.] The behavior of $\mathrm{Im}N_f g^<(\epsilon-i0^+)$ as a function of ϵ_f is therefore very different from the $N_f=1$ case except for $\epsilon_f\gg\Delta$. As ϵ_f approaches the Fermi energy from above and moves below it, a remnant of an ($N_f=1$)-like affinity peak is pinned above the Fermi energy at $\epsilon_f-\Delta E$ (see also Sec. VII) and the onset of this peak shows up in $\rho_v(\epsilon)$ [(6.23)]. The weight of this peak, which cannot be explained in a "one-particle picture," decreases like $1-n_f$ when ϵ_f moves further below ϵ_F and $\epsilon_f-\Delta E$ moves closer to ϵ_F. In the spin-fluctuation limit ($\epsilon_f\ll -N_f\Delta$), a "normal" ionization peak at ϵ_f with a width $\pi N_f V^2$ occurs in $\rho_v(\epsilon)$ (for $B\gg|\epsilon_f|$) and the relative weight of the rise at ϵ_F becomes extremely small. The drastic increase of $\rho_v(\epsilon)$ when ϵ approaches ϵ_F in the spin-fluctuation limit, has been discussed in connection with the formation of local moments ($N_f=2$).[38] In the symmetric case ($2\epsilon_f+U=0$) the spectral function of the local one-particle Green's function has a peak directly at the Fermi energy for a symmetric band as can be deduced from the particle-hole symmetry of the problem and the generalized Friedel sum rule (FSR) discussed below. This peak is usually called the "Kondo" peak. A universal expression for the shape of $\rho_v(\epsilon)$ near ϵ_F in the spin-fluctuation limit including the continuum part resulting from Img is given in Appendix C.

The increase of $\rho_v(\epsilon_F)$ with N_f as well as the accuracy of result (6.23) for finite N_f can be discussed in terms of the exact Fermi-liquid relation[39] between $\rho_v(\epsilon_F)$ and n_f, which follows from particle-number conservation ("generalized FSR").[40] We have

$$\rho_v^{\mathrm{exact}}(\epsilon_F)=\frac{N_f}{\pi\Delta}\sin^2\left[\frac{\pi n_f}{N_f}\right], \tag{6.26}$$

where it again has been assumed that the band is broad and that $V(\epsilon)$ is constant ($\Delta=\pi V^2$). In this limit result (6.23) takes the form

$$\rho_v(\epsilon_F)=\frac{\pi}{N_f\Delta}n_f^2, \tag{6.27}$$

where we have used Eqs. (3.13) and (3.17). Expanding the sin function in (6.26) we can see that expressions (6.26) and (6.27) are identical for $N_f=\infty$, as they should. In Fig. 9 we show Eqs. (6.26) and (6.27) as a function of N_f for a mixed-valence system ($n_f=0.8$) and a system in the spin-fluctuation regime.

For $N_f\geq 6$, the result [(6.27)] deviates less than 10% from the exact result even in the spin-fluctuation limit, and for $N_f=14$ the deviation is less than 2%. Figure 9 also illustrates how $\rho_v(\epsilon_F)$ grows with N_f in the limit $N_f\Delta=$const. For $n_f=0.99$ the $N_f=\infty$ result for $\rho_v(\epsilon_F)$ is about a factor $\pi^2/4\approx 2.5$ larger than the $N_f=2$ result. In Fig. 10 we compare the analytical result (6.16), and the more accurate result (6.21) for $N_f=6$. The similarity between the curves further supports the conclusion that Eq. (6.16) is quite accurate for $N_f\geq 6$. In Fig. 11 we show the quantities $\mathrm{Im}\tilde{\Gamma}(\epsilon-i0^+)$, $\mathrm{Re}\tilde{\Gamma}(\epsilon-i0^+)$, and $\epsilon-\epsilon_f$ which enter

$$\mathrm{Img}(\epsilon-i0^+)=\frac{N_f\mathrm{Im}\tilde{\Gamma}(\epsilon-i0^+)}{[\epsilon-\epsilon_f-N_f\mathrm{Re}\tilde{\Gamma}(\epsilon-i0^+)]^2+[\mathrm{Im}\tilde{\Gamma}(\epsilon-i0^+)]^2}. \tag{6.28}$$

The figure also shows $\mathrm{Img}(\epsilon-i0^+)$ and $|a(\epsilon)|^2$ which enter (6.16). The figure illustrates how the sharp cutoff in $\mathrm{Im}\tilde{\Gamma}(\epsilon-i0^+)$ leads to a logarithmic singularity in $\mathrm{Re}\tilde{\Gamma}(\epsilon-i0^+)$ and a pole in $g(\epsilon-i0^+)$. In addition there is a split-off state slightly below the bottom of the band and a large contribution to $\mathrm{Img}(\epsilon-i0^+)$ just above the bottom of the band. This leads to the peak at -2.1 eV in Fig. 11. Such a peak at the bottom of the band is to be expected if the density of states goes to zero fairly rapidly and $N_f\Delta$ is not small compared with ϵ_f+B but ϵ_f is within the band.

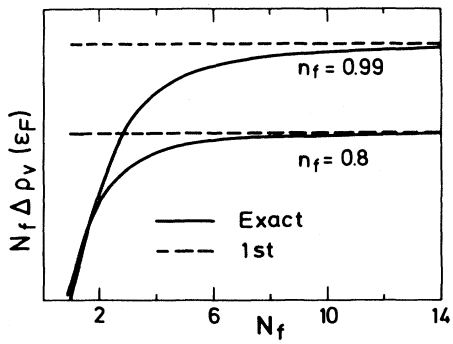

FIG. 9. Weight $\rho_v(\epsilon_f)$ of the valence spectrum at the Fermi energy as a function of the degeneracy N_f. The exact result [solid curve, Eq. (6.26)] is compared with the lowest-order result [dashed curve, (6.27)]. To make the results more universal we have multiplied them by $N_f\Delta$. Figure shows results for both the mixed-valence ($n_f=0.8$) and spin-fluctuation regimes ($n_f=0.99$).

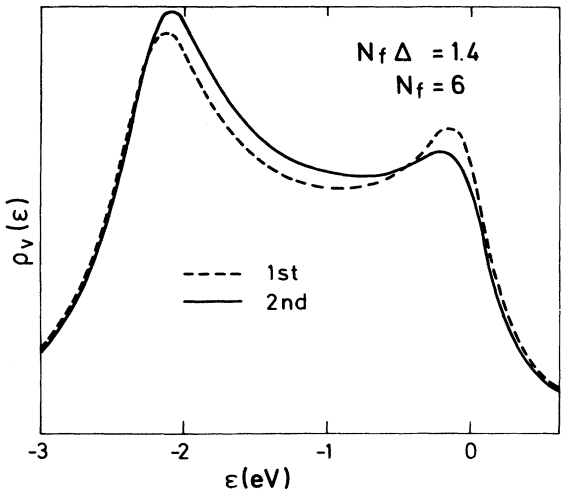

FIG. 10. Valence photoemission spectrum in the first- (dashed curve) and second- (solid curve) order treatments. We have used the parameters [Eq. (3.22)] $B=2$, $\epsilon_f=-1$, and $N_f\Delta=1.4$. Lorentzian broadening of 0.5 eV (FWHM) was introduced. All energies are in eV.

VII. BREMSSTRAHLUNG ISOCHROMAT SPECTROSCOPY

BIS, or inverse photoemission, is complementary to valence photoemission since it gives information about the unoccupied states. In particular, BIS has been used to determine the energy of the f^2 configuration, which provides an estimate of U.[16]

In BIS, electrons with a large energy make transitions into lower-lying unoccupied states in a radiative process and the energy of the emitted photon is measured. Here

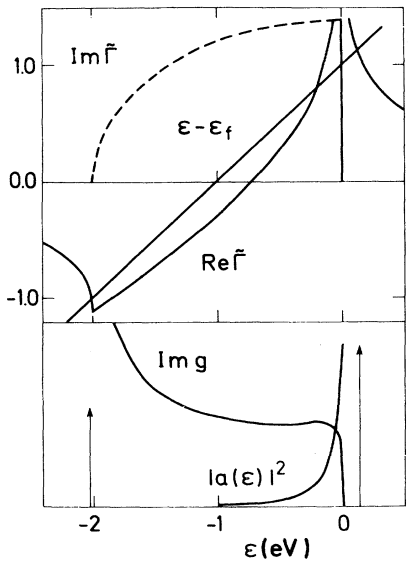

FIG. 11. Quantities Re $\tilde{\Gamma}(\epsilon-i0^+)$, Im$\tilde{\Gamma}(\epsilon-i0^+)$ [Eq. (6.15)], $\epsilon-\epsilon_f$, $|a(\epsilon)|^2$, and Img$(\epsilon-i0^+)$ [Eq. (6.14)]. Same parameters as in Fig. 10 are used.

we focus on the process where the incoming electron falls into an f orbital. This process is described by the operator

$$T=\sum_\nu \omega_\nu \psi_\nu^\dagger \psi_{\tilde{E}\nu} . \tag{7.1}$$

We assume that the initial state, with a fast incoming electron, can be written as

$$\psi_{\tilde{E}\nu}^\dagger |\phi_0\rangle . \tag{7.2}$$

The probability for observing a photon with energy ω is then

$$I(\omega)\sim\frac{1}{\pi}|\omega_\nu|^2 \times \mathrm{Im}\left\langle\phi_0\left|\psi_\nu\frac{1}{\omega-i0^+-E_0(N)-E+H}\psi_\nu^\dagger\right|\phi_0\right\rangle . \tag{7.3}$$

We therefore study the Green's function

$$g^>(z)=\left\langle\phi_0\left|\psi_\nu\frac{1}{z+E_0(N)-H}\psi_\nu^+\right|\phi_0\right\rangle , \tag{7.4}$$

which is related to $I(\omega)$,

$$I(\omega)=\frac{1}{\pi}|\omega_\nu|^2\mathrm{Im}g^>(E-\omega-i0^+) . \tag{7.5}$$

With this definition $\mathrm{Im}g^>(\epsilon-i0^+)\equiv 0$ for $\epsilon<0$, while $\mathrm{Im}g^<(\epsilon-i0^+)$, introduced for valence photoemission, is zero for $\epsilon>0$. These definitions allow us to easily compare the BIS and valence photoemission spectra.

In the calculation of the ground state $|\phi_0\rangle$ we take double occupancy of the f level into account (see Appendix B), but neglect the second-order state [Eq. (3.3)]. The latter states have a small weight and would complicate the calculation.

The choice of basis states for the inversion of the operator $[z+E_0(N)-H]$ is more difficult than for valence photoemission. The weight,

$$(N_f/\pi)\mathrm{Im}\int g^<(\epsilon-i0^+)d\epsilon ,$$

of the valence spectrum is n_f, while the corresponding weight for the BIS spectrum is N_f-n_f. An exact theory should, nevertheless, give

$$\mathrm{Im}g^>(0^+-i0^+)=\mathrm{Im}g^<(0^--i0^+) .$$

Even in the limit $N_f\to\infty$, this requires that the BIS theory is correct to order $1/N_f$, since the weight of the BIS spectrum is of the order N_f. Thus lowest-order basis functions are not sufficient in the BIS calculation. A systematic inclusion of all contributions of the order $1/N_f$ does, however, not seem worth the effort at the present stage. The choice of basis states below and the first-order ground state give, nevertheless, a continuous connection between the two spectra for $N_f=\infty$, at least if f^2 states are suppressed. For any finite N_f, there is a discontinuity at $z=0$, but this defect is usually not detectable for a realistic broadening of the spectrum. We use the basis states

$$|\nu\rangle=\psi_\nu^\dagger|0\rangle\ , \tag{7.6}$$

$$|\epsilon,\nu\rangle=\frac{1}{\sqrt{N_f-1}}\sum_{\nu'\neq\nu}\psi_\nu^\dagger\psi_{\nu'}^\dagger\psi_{\epsilon\nu'}|0\rangle\ , \tag{7.7}$$

$$|E,\nu\rangle=\psi_{E\nu}^\dagger|0\rangle\ , \tag{7.8}$$

$$|E,\epsilon,\nu;1\rangle=\frac{1}{\sqrt{N_f-1}}\sum_{\nu'\neq\nu}\psi_{E\nu}^\dagger\psi_{\nu'}^\dagger\psi_{\epsilon\nu'}|0\rangle\ , \tag{7.9}$$

$$|E,\epsilon,\nu;2\rangle=\frac{1}{\sqrt{N_f-1}}\sum_{\nu'\neq\nu}\psi_{\nu}^\dagger\psi_{E\nu'}^\dagger\psi_{\epsilon\nu'}|0\rangle\ , \tag{7.10}$$

$$|E,\epsilon,\nu;3\rangle=\psi_{E\nu}^\dagger\psi_{\nu}^\dagger\psi_{\epsilon\nu}|0\rangle\ , \tag{7.11}$$

Although BIS and XAS (Sec. V) are formally very similar, our larger demand on the accuracy of the BIS calculation requires a larger basis set [(7.6)–(7.11)] and therefore a separate treatment. Using a similar technique as used for the other spectroscopies (see, e.g., Appendix E), we calculate the matrix elements of

$$[z+E_0(N)-H]\equiv[G^>(z)]^{-1}$$

and invert the corresponding matrix. This approach yields

$$g^>(z)=\sum_{i=0}^{N}\sum_{j=0}^{N}a_i^*G_{ij}^>(z)a_j\ , \tag{7.12}$$

where

$$a_0=A\ ,$$

$$a_i=A[w_i(N_f-1)/N_f]^{1/2}a(\epsilon_i)\ .$$

The matrix $G^>(z)$ is obtained by inverting

$$(G^>)_{00}^{-1}=z+\Delta E-\epsilon_f-\mu_0(z)\ , \tag{7.13}$$

$$(G^>)_{0i}^{-1}=-\sqrt{N_f-1}V(\epsilon_i)[1+\mu_1(z,\epsilon_i)]\sqrt{w_i},\quad 1\le i\le N \tag{7.14}$$

$$(G^>)_{ij}^{-1}=z+\Delta E-2\epsilon_f-U+\epsilon_i+2\gamma(-z-\Delta E+\epsilon_f-\epsilon_i)\delta_{ij}+(N_f-1)\frac{V(\epsilon_i)V(\epsilon_j)}{\epsilon_i-\epsilon_j}[\mu_1(z,\epsilon_i)-\mu_1(z,\epsilon_j)]\sqrt{w_iw_j}\ ,$$

$$1\le i,j\le N\ . \tag{7.15}$$

We have discretized the occupied part of the conduction band $(-B,0)$ in N points, ϵ_i, as in Appendix E, and introduced the weight factors w_i [see the text after Eq. (E3)]. We have also defined the function

$$\mu_n(z,\epsilon)=\int_0^\infty\frac{|V(E)|^2}{(z+\Delta E-E-\epsilon_f+\epsilon)^n(z+\Delta E-E+N_f\tilde{\Gamma}(-z-\Delta E+E+\epsilon_f)}dE\ . \tag{7.16}$$

Since $\mu_0(z,\epsilon)$ is independent of ϵ, we use the notation $\mu_0(z)$. The functions $\tilde{\Gamma}(z)$ and $\gamma(z)$ are defined in Eqs. (6.15) and (E.7), respectively.

A typical spectrum is shown in Fig. 12. There is one peak at $\sim\epsilon_f-\Delta E$ due to a transition to an f^1 final state, and another peak at $\sim 2\epsilon_f+U-\Delta E$ corresponding to an f^2 final state. The f^2 peak is mainly due to matrix element (7.15). This element contains an imaginary part $2\,\mathrm{Im}\gamma\sim 2\pi V^2$, which describes how an f^2 state can decay through the tunneling of either of the two f electrons into a conduction state. We observe the difference from the valence photoemission spectrum. Since the hole created in the photoemission process can be filled in N_f ways, the corresponding imaginary part of the ionization peak at ϵ_f ($\ll -N_f\pi V^2$) is $N_f\pi V^2$. The f^2 peak in the BIS spectrum shows a tailing towards higher energies. The reason is that the final state contains two f electrons and one hole in the conduction band. This hole is likely to be close to the Fermi energy, but can also be located further down, which corresponds to the high-energy tail of the f^2 peak. Because of this tailing, the f^2 peak appears broader than one would expect from the imaginary part of Eq. (7.15). This is in particular the case if the f occupancy is small.

To study the f^1 peak in more detail, we assume $U=\infty$, which allows us to obtain an analytical solution. This yields

$$g^>(z)=(1-n_f)\frac{1}{z+\Delta E-\epsilon_f-\mu_0(z)}\ , \tag{7.17}$$

where $\mu_0(z)$ is defined in Eq. (7.16). We can rewrite the integrand of Eq. (7.16) for $n=0$ as

$$\frac{|V(E)|^2}{z+\Delta E-E+N_f\tilde{\Gamma}(-z-\Delta E+E+\epsilon_f)}=\frac{(1-n_f)|V(E)|^2}{z-E}+\tilde{\mu}(z-E)\ , \tag{7.18}$$

where

$$\mathrm{Im}\tilde{\mu}(\epsilon-i0^+)=0\ \text{ for }\epsilon<\epsilon_f-\Delta E\ . \tag{7.19}$$

The determination of the strength of the pole at $z=E$ in Eq. (7.18) is quite analogous to the calculation in Eq. (6.22). We then obtain

$$\mathrm{Im}\mu_0(\epsilon-i0^+)=(1-n_f)\pi|V(\epsilon)|^2,\quad 0\le\epsilon<\epsilon_f-\Delta E\ . \tag{7.20}$$

This leads to a small broadening of the f^1 peak, in particular if $n_f\sim 1$. For $N_f\to\infty$ and $0<\epsilon<\epsilon_f-\Delta E$ we can expand the imaginary part of (7.17) as

$$\frac{1}{\pi}\mathrm{Im}N_fg^>(\epsilon-i0^+)=\frac{(1-n_f)^2}{(\epsilon+\Delta E-\epsilon_f)^2}N_f|V(\epsilon)|^2\ . \tag{7.21}$$

This joins smoothly to the valence photoemission spectrum, Eq. (6.23), at $\epsilon=0$, as it should. For a finite value of N_f, Eq. (7.17) has a pole at a slightly negative ϵ and

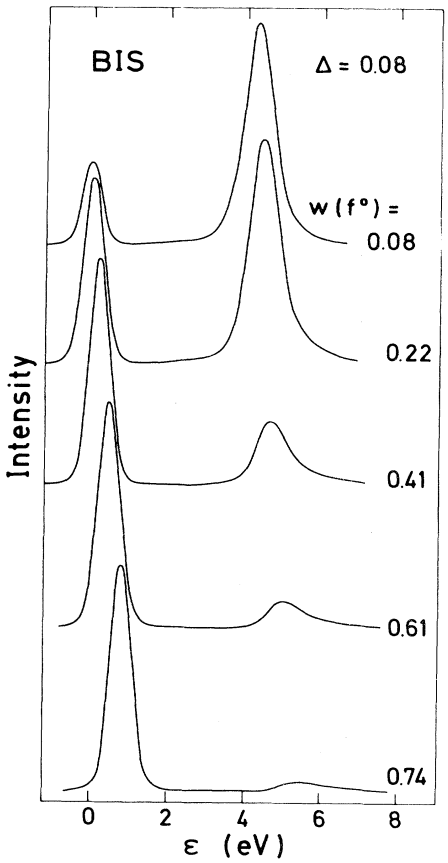

FIG. 12. BIS as a function of the f^0 weight $w(f^0)$ in the initial state. Peaks are normalized to the height of the larger peak and the energy zero is at ϵ_F. We have used the parameters [Eq. (4.10)] $\epsilon_0=-1.22$, $B=2.79$, and $\epsilon_f+U=4$ eV and introduced a Gaussian broadening of 0.65 eV (FWHM).

there is a discontinuous connection between the valence photoemission and BIS spectra. This unphysical result is due to a slightly inconsistent choice of basis states for the final and initial states. This inconsistency is not very aesthetic from a theoretical point of view and indicates the problems one encounters in the attempt of a unified $1/N_f$ expansion for *both* $g^<$ *and* $g^>$ but this complication is, however, normally not visible if realistic broadening is taken into account. For instance, we used a constant $|V(\epsilon)|^2$ with $\Delta=0.12$ eV, $N_f=14$, $B=2$, and $\epsilon_f=-1.6$, which leads to $n_f=0.85$. In this case the pole of (7.17) was less than 10^{-4} eV below ϵ_f and had a weight smaller than 0.01.

In Fig. 7 we show the weight of the f^1 peak as a function of $w(f^0)$, the weight of the f^0 configuration in the initial state. Since in BIS an f electron is added to the system, there is relation between these two quantities. We now compare the XPS, XAS, and BIS results in Fig. 7. To understand these results, we first consider the model of Fig. 1 and for simplicity we write the ground state as

$$|\phi_0\rangle=c_0|f^0\rangle+c_1|f^1\rangle\ . \tag{7.22}$$

If the hopping integral between $|f^0\rangle$ and $|f^1\rangle$ is negative, c_0 and c_1 have the same sign since $|\phi_0\rangle$ is the ground state. The f^0 peak in the XPS spectrum corresponds to the final state

$$|\tilde{f}^0\rangle=c_0^1|f^0\rangle+c_1^1|f^1\rangle\ , \tag{7.23}$$

where we have suppressed the occupation number of the core level and assumed that the weight of f^2 is negligible. The weight of the f^0 peak is then [see Eq. (1.1)]

$$p_0=|c_0c_0^1+c_1c_1^1|^2\ .$$

Since the final $|\tilde{f}^0\rangle$ state is higher in energy than the final $|\tilde{f}^1\rangle$ state, c_0^1 and c_1^1 have different signs. It then follows that

$$p_0<|c_0|^2=w(f^0)\ . \tag{7.24}$$

The coupling between the f^0 and f^1 configurations is $N_f\Delta\lesssim 2$ eV. This is much smaller than the energy separations between these configurations in the final state, ~ 11 eV. The coefficient c_1^1 is therefore small and c_0^1 is close to 1. This explains why p_0 and $|c_0|^2=w(f^0)$ are similar. We can use similar arguments for $3d\rightarrow 4f$ XAS, except that the final f^1 and f^2 configurations now serve the same purpose as f^0 and f^1 did for XPS. Since, however, the energy separation between the final f^1 and f^2 configurations is smaller (~ 5 eV) the deviation between $w(f^0)$ and the weight of the f^1 peak is larger. BIS is similar to XAS in this respect, except that there is no core hole for BIS. The final f^2 configuration is therefore higher in energy than the f^1 configuration. This means that for the f^1-like final state,

$$|\tilde{f}^1\rangle=c_1^1|f^1\rangle+c_2^1|f^2\rangle\ , \tag{7.25}$$

the coefficients c_1^1 and c_2^1 have the same sign and the matrix element, $|\langle\tilde{f}^1|\psi_v^\dagger|\phi_0\rangle|^2$ is larger than $|c_0|^2=w(f^0)$.

We can now discuss both the "occupied" and "unoccupied" parts of the valence spectrum. To illustrate the strong correlation effects, we show in Fig. 14 both a spectrum with correlation effects included and spectrum in the Hartree-Fock approximation. In the latter we have chosen the position of the effective level

$$\epsilon_f+U(N_f-1)\langle n_f\rangle/N_f$$

in such a way that the f occupancy becomes the same as for the correlated spectrum. The correlated spectrum has been obtained from Eqs. (6.21) ($\epsilon<0$) and (7.12)–(7.16) ($\epsilon>0$). We have introduced a Lorentzian broadening of 0.6 eV full width at half-maximum (FWHM), as the peak amplitudes otherwise differ so drastically that it is hard to represent them in one figure.

The figure illustrates the variation in the number of peaks with ϵ_f. For ϵ_f far above ϵ_F, the f level is empty and there is only a BIS f^1 peak, which in this situation is very similar to the Hartree-Fock (HF) peak. As ϵ_f is moved down, the f level is partly occupied and the spectrum acquires a second peak, the BIS f^2 peak. This is illustrated by the two uppermost curves in Fig. 13. If ϵ_f is moved even further down a third peak develops, the

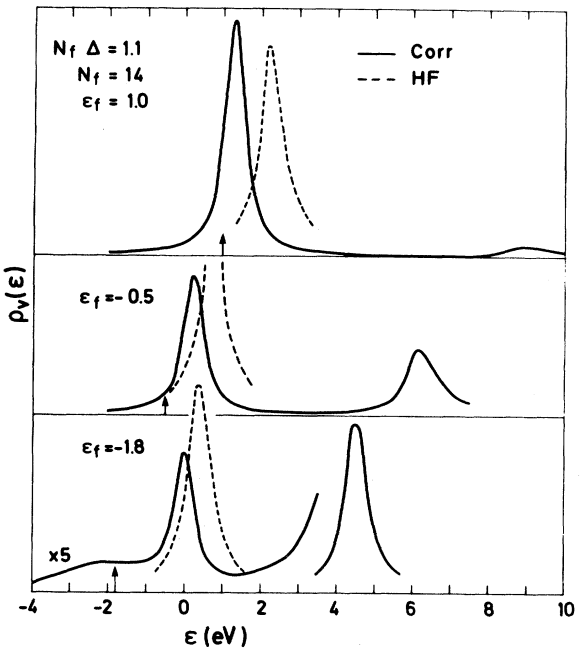

FIG. 13. Combined photoemission and BIS spectra with a Lorentzian broadening (0.6 eV FWHM). Figure shows the spectrum with correlation taken into account (solid curve) and in the HF approximation (dashed curve). In the latter case, the effective level has been placed so that the *unbroadened* interacting and noninteracting curves have the same weight below ϵ_F in each panel. Observe that the left, lower, interacting curve has been multiplied by a factor of 5. Parameters are $U=6$ eV, $N_f\Delta=1.1$ eV, $N_f=14$, $\epsilon_0=-1.22$ eV, and $B=2.79$ eV [Eq. (4.10)]. Equation (4.10) has been slightly modified above ϵ_F so that $V(\epsilon)^2$ is never smaller than 0.1 times its maximum value. Arrows show the positions of the f level.

photoemission f^0 peak (see the lower spectrum). (Compare to the discussion in Sec. VI.) The HF spectrum has, of course, only one peak, unless Δ is much larger than the values used here (no split-off states). It is also interesting to compare the widths of the peaks. While the HF peak has a half-width $\sim\Delta$, the peak widths in the correlated spectrum are quite different for the different peaks and they can also depend on the value of n_f. The shape of the lower peak in the photoemission spectrum depends on the large quantity $N_f\Delta$, while the higher peak (the onset of the BIS f^1 peak) grows on the energy scale $\epsilon_f-\Delta E$. The BIS f^1 peak tends to have a half-width $(1-n_f)\Delta$ [Eq. (17.20)] and the BIS f^2 peak obtains a half-width 2Δ due to tunneling into the conduction states. For the latter peak the tailing towards higher energies can give an important additional contribution to the width, in particular if n_f is small. In the spin fluctuation limit $\epsilon_f \ll -N_f\Delta$ and for a large U the relative weights of the three peaks are as follows: The ionization peak near ϵ_f has the weight $n_f\approx 1$, the weight of the f^1 peak (Kondo peak) at $\epsilon_f-\Delta E\approx 0$ is $(1-n_f)N_f$ and the f^2 peak near $2\epsilon_f+U-\Delta E$ has a weight $n_f(N_F-1)\approx N_f-1$. Therefore even for $n_f=0.9$ and $N_f=14$ the weight of the f^1 peak is larger than the weight of the ionization peak: Even if there is a small chance, $1-n_f$, to find the f level empty, there are N_f different ways to put in the extra electron. From this argument it can also be inferred that only a fraction $\sim 1/N_f$ of the f^1 peak is seen in photoemission. Almost all its weight lies on the BIS side for large degeneracy N_f. To show this fact in a figure like Fig. 13, we would have to chose a broadening smaller than $\epsilon_f-\Delta E$. Since this f^1 peak then would be extremely high and narrow, an extreme spin-fluctuation case is not included in Fig. 13.

VIII. STATIC $T=0$ SUSCEPTIBILITY

Ce compounds often have a large susceptibility, which, however, varies strongly between different compounds.[1-3] The large susceptibility is ascribed to the f electrons, and it has been assumed to imply a small value of Δ.[4] Below we analyze the static $T=0$ susceptibility in the impurity model. For the susceptibility it is important to take the spin-orbit coupling into account to describe the coupling to the external magnetic field κ. The Hamiltonian (2.1) is therefore replaced by

$$H=\sum_{k,\sigma}\epsilon_k n_{k\sigma}+\sum_{\nu=1}^{2}\sum_{m=-j_\nu}^{j_\nu}(\epsilon_\nu-g_\nu\mu_B m\kappa)n_{\nu m}+\sum_{\nu=1}^{2}\sum_{k,m,\sigma}(V_{km\sigma}^{j_\nu}\psi_{\nu m}^{\dagger}\psi_{k\sigma}+\text{H.c.}), \tag{8.1}$$

where $j_1=\frac{5}{2}$ and $j_2=\frac{7}{2}$ are the two spin-orbit-split f levels, and ϵ_ν are the corresponding energies. Landé's g factor is given by g_ν and μ_B is the Bohr magneton. The hopping parameters $V_{km\sigma}^{j_\nu}$ can be expressed in the parameter introduced earlier, V_{km}, by using the relations[41] between the states $|jm\rangle$ and $|l_z\sigma\rangle$. We assume that double occupancy of the f level can be neglected and the Coulomb interaction is therefore not shown explicitly in (8.1).

To obtain the susceptibility, we calculate the total energy at $T=0$ and differentiate twice with respect to the external magnetic field κ. Performing a variational calculation as in Sec. III, we obtain

$$\Delta E(\kappa)=\sum_{\nu,m}\int d\epsilon\frac{|V(\epsilon)|^2}{\Delta E(\kappa)-\epsilon_\nu+g_\nu\mu_B m\kappa+\epsilon_k+\gamma[-\Delta E(\kappa)-\epsilon]}, \tag{8.2}$$

where γ is defined in Eq. (E7). This leads to the susceptibility

$$\chi=-\tfrac{2}{3}\mu_B^2\frac{\sum_\nu g_\nu^2 j_\nu(j_\nu+1)G_3^\nu(\Delta E)}{1-\sum_\nu\frac{\partial}{\partial(\Delta E)}G_1^\nu(\Delta E)}, \tag{8.3}$$

where

$$G_n^\nu(\Delta E)=\int d\epsilon\frac{|V(\epsilon)|^2(2j_\nu+1)}{[\Delta E-\epsilon_\nu+\epsilon+\gamma(-\Delta E-\epsilon)]^n}. \tag{8.4}$$

For the discussion, we now work to lowest order in $1/N_f$

and drop the second-order term γ. We also neglect the $j_2=\frac{7}{2}$ level for a moment, although this is not a good approximation (see Appendix A). If we further assume that $N_f|V(\epsilon)|^2$ is constant and much smaller than B, where $-B$ is the bottom of the band, we obtain

$$\chi=\frac{1}{3}\frac{j_1(j_1+1)}{2j_1+1}g_1^2\mu_B^2\frac{\pi}{\Delta}\frac{n_f^2}{1-n_f}\ . \tag{8.5}$$

The susceptibility has been calculated to this accuracy by several groups,[35,31] and it can be written in different ways. We have here preferred a form which shows explicitly the dependence on n_f and Δ since these are the parameters which interest us in particular. Alternatively, one could express (8.5) in terms of $|\epsilon_f-\Delta E|$, which is the Kondo temperature for $n_f\to 1$. We write

$$\chi=\tfrac{1}{3}j_1(j_1+1)g_1^2\mu_B^2\frac{n_f}{|\Delta E-\epsilon_f|}\ . \tag{8.6}$$

The expression for χ obtained by Newns and Hewson[4] could also be written in the form (8.5), except for the factor $(1-n_f)^{-1}$.

Equation (8.5) indicates that if we know one of the quantities n_f and Δ, in addition to the experimental susceptibility, we can deduce the other one. For instance, one can use

$$\Delta\sim\frac{1}{\chi}\frac{n_f^2}{1-n_f}\ , \tag{8.7}$$

and insert the experimental value of χ and an estimate of n_f to obtain a value of Δ. However, Eq. (8.7) illustrates that Δ then depends very sensitively on n_f and the method is only useful if we know n_f quite accurately. If we have an estimate of Δ, it is much more favorable to use the susceptibility for an estimate of n_f. For typical parameters, an error in our value for Δ or χ of a factor of 2 leads to an error in the estimate of n_f of less than 0.1.

For quantitative calculations it is important to include spin-orbit splitting instead of using the simple formula (8.5). In Fig. 14 we show some typical results. To obtain an idea of the accuracy we consider both the first- and second-order theories which give similar results. The difference between the first- and second-order theories is, however, somewhat larger if χ is shown as a function of ϵ_f. Also in the presence of spin-orbit splitting there is a very strong dependence on n_f, comparable to Eq. (8.5). Equation (8.5) is, however, not very accurate when spin-orbit splitting is included, as illustrated by the crossing of the $\Delta=0.12$- and the 0.03-eV curves.

IX. LATTICE-PARAMETER DATA

The f occupancy in rare-earth compounds has often been estimated from lattice-parameter data.[1-3] The lattice parameters of hypothetical compounds with $n_f=1$ and 0 are estimated and it is assumed that the lattice parameter varies *linearly* with n_f. Knowing the lattice parameter of the real system one can then estimate the value of n_f. This method can be problematic both in terms of estimating the lattice parameter of the hypothetic compounds and the assumption of a linear dependence on n_f. We want to address the latter issue for Ce compounds.

For Ce compounds we find a fairly large value for the hybridization Δ so that the f level contributes to the cohesion. Since the hopping matrix elements $V(\epsilon)$ increase when the lattice parameter is reduced the f contribution to the cohesion grows. This corresponds to a contractive force on the lattice due to the f electrons. This force depends, however, on the f occupancy. If n_f is small, i.e., ϵ_f is far above ϵ_F, the force is small. The same is normally true if $n_f\approx 1$, since then typically $\epsilon_f\ll\epsilon_F$ but $U+\epsilon_f\gg\epsilon_F$, so that hopping from the f^1 configuration into both the f^0 and the f^2 configuration is small, and the f contribution to cohesion is rather independent of $V(\epsilon)$. The force due to the f electrons,

$$\frac{d(\Delta E)}{da}=\frac{dV(a)}{da}\frac{d(\Delta E)}{dV}\ , \tag{9.1}$$

is therefore small. We have assumed that the hopping matrix element $V(\epsilon)$ [Eq. (2.2)] has a separable "a" dependence $V(\epsilon,a)=V(a)F(\epsilon)$. The contraction of the lattice due to the f cohesion is largest for $n_f\sim 0.5$. This contribution should be added to other effects, e.g., the contraction of the Ce ion when n_f is reduced, and it tends to give a nonlinear dependence on n_f. The neglect of this nonlinear dependence leads to an underestimate of n_f.

To obtain a more quantitative estimate we have calculated $d(\Delta E)/dV$. To determine the contraction, we write the total energy of the system as

$$E(a_0)+\tfrac{1}{2}\frac{\partial^2 E}{\partial a^2}(a-a_0)^2+\Delta E(a_0)+\frac{\partial(\Delta E)}{\partial a}(a-a_0)\ , \tag{9.2}$$

where we have assumed that the energy and the lattice parameter would be $E(a_0)$ and a_0, respectively, if the f elec-

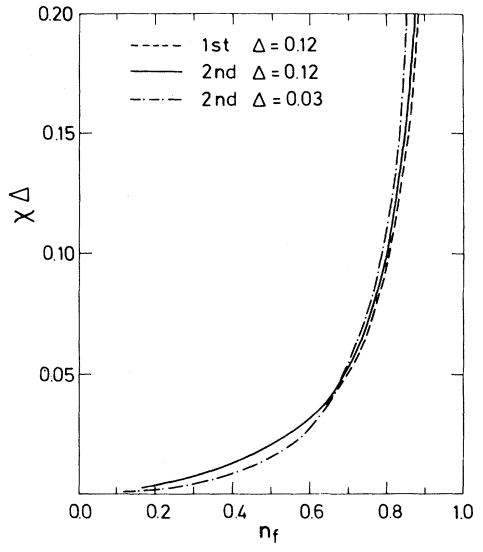

FIG. 14. Susceptibility χ multiplied by Δ as a function of n_f. Spin-orbit splitting is taken into account. Figure compares the first- (dashed curve) and second- (solid curve) order calculation for $\Delta=0.12$ and the result for $\Delta=0.12$ (solid curve) and $\Delta=0.03$ (dashed-dotted curve). Parameters are [Eq. (3.22)] $B=3$ eV and $\Delta\epsilon_f=0.25$ eV. Double occupancy of the f level is neglected.

trons did not contribute to the cohesion. We can then estimate the f-electron-induced contraction as

$$a-a_0=-\left[\frac{\partial^2 E}{\partial a^2}\right]^{-1}\frac{\partial(\Delta E)}{\partial a}\ . \tag{9.3}$$

We relate $\partial^2 E/\partial V^2$ to the experimental bulk modulus and use Eqs. (9.1) and (9.2). For $V(a)$ we assume a power dependence on a,

$$V(a)=(a_0/a)^{\nu}V_0\ . \tag{9.4}$$

Using the bulk modulus of α-Ce we obtain the results shown in Fig. 15 where we have expressed $(a-a_0)/a_0$ in terms of the power ν in Eq. (9.4). According to arguments from the linear muffin-tin method,[42] one may expect the hopping matrix element to vary with the power $\nu=6$. However, the definition (2.2) of $V(\epsilon)$ also involves the density of states, which partly compensates for the variation of the hopping matrix element. This makes it hard to give an accurate estimate of ν, and we leave its value open. Figure 15 shows, however, that $(a-a_0)/a_0$ may be of the same order as the relative difference (0.1) between hypothetical Ce metals with $n_f=0$ and 1. The assumption that a has a linear variation with n_f may therefore lead to a large error in the estimate of n_f.

Even for $w(f^0)\approx 0$ there is a substantial f contribution to the force. This is partly due to the f^2 configuration. For instance, $w(f^0)=0.03$ corresponds to $\epsilon_f=-1.5$ eV for the parameters in Fig. 15. The energy separation between the f^1 and f^2 configurations is 3.5 eV and hopping into the f^2 configuration starts to become important.

Finally, we note that the calculations in Fig. 15 are performed for a nonmagnetic state where the hopping between the f^0 and f^1 configuration is determined by $N_f\Delta$. The intersite interaction, not included in model (2.1), can lead to a magnetic ground state where on each site one of the N_f f levels is preferentially occupied. In this case the hopping between the f^0 and f^1 configurations is partly determined by the much smaller quantity Δ [see Appendix F and also Eq. (A1)], and the force due to the f cohesion is reduced.

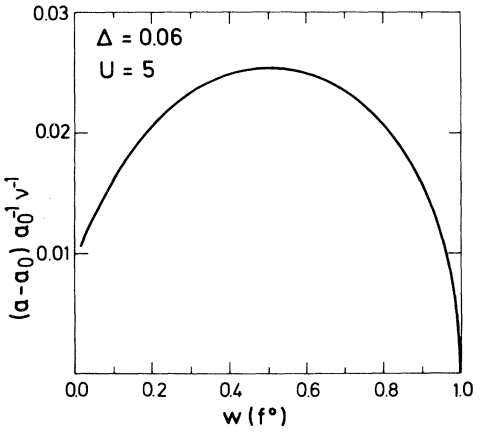

FIG. 15. Relative change $(a-a_0)a_0^{-1}$ of the lattice parameter caused by the f contribution to the cohesion as a function of the weight $w(f^0)$ of the f^0 configuration in the initial state. Calculated result has been divided by the parameter ν [Eq. (9.4)]. We have used the bulk modulus of α-Ce and the parameters $\Delta=0.06$ eV, $B=2$ eV, and $U=5$ eV together with the band structure [(3.22)].

X. APPLICATIONS

We now apply the theory presented in the preceding sections to $CeNi_2$, for which there are core-level XPS,[21] $3d\rightarrow 4f$ XAS,[20] BIS,[22] and static $T=0$ susceptibility[43] data available. $CeNi_2$ is interesting since it has traditionally been assumed to be an $n_f=0$ compound.[5] In Fig. 16 the $3d$ core spectrum is shown. We have superimposed two theoretical spectra with the weights 0.4 and 0.6 and the energy separation 18.6 eV to describe the effect of the

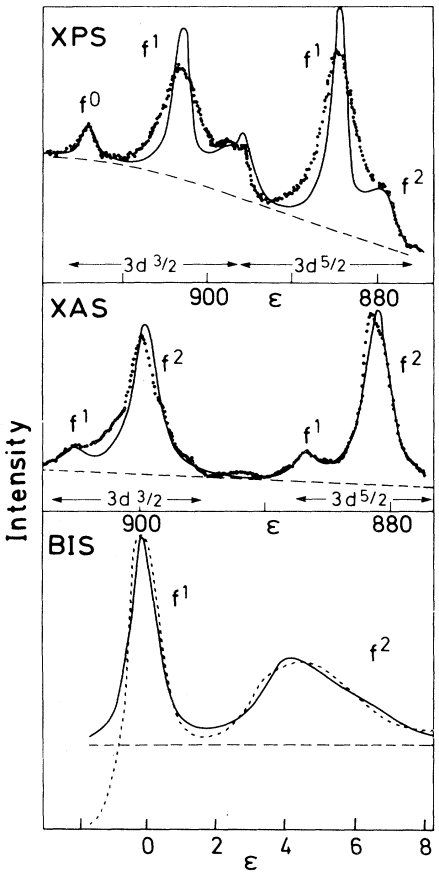

FIG. 16. $3d$ core-level XPS, the $3d\rightarrow 4f$ XAS, and the BIS spectra for $CeNi_2$. To simulate the $3d$ spin-orbit splitting we have superimposed two theoretical curves for the XPS and XAS spectra, and to describe the f^2 multiplets in the BIS spectrum we have superimposed theoretical curves with different values of U. Value of $w(f^0)$ is 0.19 (XPS), 0.23 (XAS), and 0.25 (BIS). Density of states of Eq. (4.10) was used with the parameters $\epsilon_0=-1.995$ eV, $B=2.005$ eV, and $\Delta=0.13$ eV. We used the parameters $U_{fc}=10.3$ eV, $\epsilon_f=-1.3$ eV (XPS), -1.2 eV (XAS), and -1.2 eV (BIS). Values 5.5 and 6.1 eV were used for U in the XPS and XAS spectra and the average value 5.3 eV was used for the BIS calculation.

$3d$ spin-orbit splitting, which is not included in the model. An inelastic background has also been added to the calculated spectrum. For $|V(\epsilon)|^2$ we use model (4.10), with $\epsilon_0=-1.995$ eV and $B=2.005$ eV, which gives a small density of conduction states at ϵ_F as is observed experimentally. The value of V (or Δ) was adjusted so that the experimental weight of the $3d_{5/2}f^2$ peak was reproduced, and $\epsilon_f(n_f)$ was varied until the weight of the $3d_{3/2}f^0$ peak agreed with experiment. The $3d_{3/2}f^2$ and $3d_{5/2}f^0$ peaks overlap and cannot easily be used to estimate Δ and n_f. The experimental f^1 peaks appear broader than the calculated ones because the configuration with a $3d$ hole and a f electron has several lines. These multiplet effects are not included in model (2.1).

Figure 16 also shows the $3d\rightarrow 4f$ XAS spectrum. The experimental spectrum deviates from the simple 4:6 ratio for the weights of the $3d_{3/2}$ and $3d_{5/2}$ parts because of the effects of intermediate coupling.[44] We have therefore superimposed two calculated spectra and adjusted the relative weight of the $3d_{3/2}$ and $3d_{5/2}$ parts of the spectra to fit the experiment. This is less important since we are interested in the relative weights of the f^1 and f^2 peaks. We have also added a weak background as indicated. The f^2 peak clearly shows a multiplet structure not included in model (2.1). To describe the f^1-f^2 peak separation, we have increased U slightly from 5.5 eV (XPS) to 6.1 eV (XAS). This difference could be due to the different weighting of the multiplet lines in the two spectroscopies. We have also changed ϵ_f slightly to reduce the f occupancy by 0.04, which gives a better agreement with the experimental weights for the f^1 and f^2 peaks. The other parameters are unchanged. To describe lifetime broadening and instrumental resolution a Lorentzian broadening (1.8 eV, FWHM) was introduced for both the XAS and XPS spectra. Finally, Fig. 16 shows the BIS. The f^2 multiplet splitting leads to a substantial broadening of the f^2 peak, which makes a comparison of the experimental and theoretical peak weights and shapes more difficult. We have therefore added calculations using different values of U. Since the energy of the f^2 peak grows linearly with U, this procedure allows us to simulate the multiplet splitting. We used the same separations between the different f^2 lines and the same relative intensities as Lang *et al.*[16] used for γ-Ce, while the f^1-f^2 energy separation and the relative weights of the f^1 and f^2 peaks are determined by the calculation. The experimental spectrum seems to have a fairly constant background extending down to ϵ_F. Such a constant background is also observed for many systems with no f peaks close to ϵ_F, and we therefore assume that it is due to transitions into low-lying conduction states. Since such transitions are not included in the theory, a constant background has been added to the calculated curve. We have also introduced Gaussian broadening describing the instrumental resolution and energy-dependent Lorentzian broadening, $2\Gamma(\epsilon)=0.50+0.2(\epsilon-\epsilon_F)$ eV, where ϵ is the energy of the state considered. We expect lifetime effects to give a broadening which grows linearly with $\epsilon-\epsilon_F$ for small $\epsilon-\epsilon_F$. This is probably at least an important contribution to the energy-dependent part of $\Gamma(\epsilon)$, which is the same as the one used by Lang *et al.*[16] The f^1 peak also appears broader because of the $4f$ spin-orbit splitting, which is not included in the theory but simulated by $\Gamma(\epsilon\approx 0)$ which is nonzero. These two effects, however, may not fully justify the $\Gamma(\epsilon)$ used and there is a need for further study of the peak widths. Both the broadening and the background lead to substantial uncertainties in the comparison of the experimental and theoretical peak weights, and the BIS estimates of n_f appear less reliable than those obtained from XPS and XAS. The empirical broadening $2\Gamma(\epsilon)$, described above, has been introduced to minimize this uncertainty.

We have also applied the theory of Sec. VIII and calculated the susceptibility of $CeNi_2$ using the Δ obtained from XPS. The results are shown in Fig. 17. Since double occupancy is not included in the susceptibility calculation, we show the results as a function of $w(f^0)$ rather than $n_f=w(f^1)+2w(f^2)$, where $w(f^n)$ is the weight of the f^n configuration in the initial state. Comparison with the experimental susceptibility[45] gives us an estimate of $w(f^0)$. This estimate is compared with the results from the XPS, XAS, and BIS spectra in Table I. Results[23,22] for some other systems are also shown. All spectroscopies give similar estimates even if the BIS result sometimes can be about 0.2 larger than the other ones. In all cases, however, $w(f^0)$ is much smaller than 1, while $CeNi_2$, $CeNi_5$, and often $CeRu_2$ had traditionally been assumed to have $w(f^0)=1$ ($n_f=0$). To obtain an accurate description of the peak separations, we had to use slightly different values of U for the BIS (5.3 eV), XPS (5.5 eV), and XAS (6.1 eV) spectra of $CeNi_2$. We expect U to be somewhat larger in the presence of a core hole (XPS and XAS) than without a core hole (BIS). The apparent variation of U is, however, probably also due to multiplet splitting and other effects not included in the model. Our values of U for

TABLE I. f-level hybridization Δ and the weight $w(f^0)$ of the f^0 configuration in the initial state, as deduced for the XPS, the $3d$ XAS, the BIS, and the static $T=0$ susceptibility (χ). The density of states of Ref. 23 was used and an average Δ defined in Ref. 23 is shown since $V(\epsilon)^2$ has strong variations in several cases.

	Δ_{av} (eV)	$w(f^0)$			
	XPS	XPS	$3d$ XAS	BIS	χ
$CeRu_2$	0.10	0.21		0.45	0.26
$CePd_3$	0.11	0.13	0.18	0.08	0.22
$CeNi_2$	0.10	0.19	0.23	0.25	0.30
$CeNi_5$	0.09	0.24	0.22	0.42	

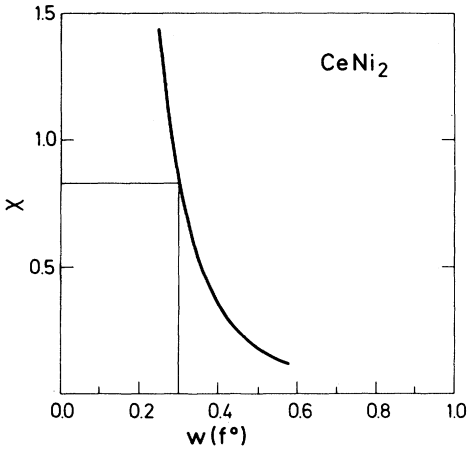

FIG. 17. Second-order [(8.3)] susceptibility χ as a function of $w(f^0)$. We have used the parameters of Fig. 16 and the spin-orbit splitting $\Delta\epsilon_f=0.25$ eV. Susceptibility is given in units of 10^{-3} emu/mole and experimental result 0.83×10^{-3} emu/mole was taken from Ref. 43.

$CeNi_2$ are fairly close to the value of 5 eV obtained for Ce by Herbst *et al.*[24] in an *ab initio* calculation, while for $CePd_3$ ($U=7.5$ eV) and $CeRu_2$ ($U=7$ eV) somewhat larger values were required to describe the core spectra. Our values of U_{fc} for $CeNi_2$ (10.3 eV), $CeNi_5$ (10.7 eV), $CeRu_2$ (10.8 eV), and $CePd_3$ (11.0 eV), which only enter the XPS and XAS calculations, are close to the result 10.3 eV obtained by Herbst and Wilkins[24] for Ce. Our values for Δ are about an order of magnitude smaller than those obtained by Oh and Doniach.[30] The reason is that the weight of the f^2 peak depends on $(N_f-1)\Delta$ [see Eqs. (E6) and (B3) and the discussion above Eq. (4.10)] since there are (N_f-1) ways of going from the f^1 to the f^2 configuration. Since Oh and Doniach used $N_f=2$ while we use $N_f=14$ one would expect their values to be about 13 times larger than ours.

XI. CONCLUDING REMARKS

We have presented a simple method for calculating the expectation value of a resolvent operator [Eq. (1.3)] for a generalized impurity Anderson model. The results are quite accurate for $N_f\geq6$, as indicated by Figs. 3, 5, 9, and 10. We have shown how this method can be used to calculate the core-level XPS, the $3d\rightarrow4f$ XAS, the valence photoemission, and the BIS spectra. Our approach can be extended to the two-impurity problem but is not well suited for a lattice of f levels. The core-level XPS spectra provide a useful method for estimating the hybridization Δ between the f state and the conduction states. We can furthermore use the XPS, XAS, and BIS spectra to estimate n_f. This is summarized in Fig. 7. XPS is particularly favorable since the weight of the $3d_{3/2}f^0$ peak is closely related to $w(f^0)$. For $3d\rightarrow4f$ XAS and BIS we have to rely more on the calculations to estimate n_f, and it is harder to determine the weight of the experimental peaks because of the larger overlap. In BIS the broadening of the peaks and the large background pose particular problems in this respect. On the other hand, XPS has a larger surface sensitivity and may measure slightly different properties. It would be useful to extend the theory to ($2p\rightarrow5d$) XAS, where the peaks have a fairly large energy separation, so that the mixing of the final states should be rather small. In terms of Fig. 7, $2p$ XAS may therefore be similar to XPS, but it is less surface sensitive. To make the treatment of $2p$ XAS meaningful, one should, however, extend the model used here.

In the Introduction we mentioned the possibility that the parameters in the Anderson model may be renormalized, for instance, due to electron-phonon coupling in a different way for "low-" and "high-" energy experiments. In addition to the (high-energy) spectroscopies, we have therefore also studied the static $T=0$ susceptibility. For the mixed-valence Ce compounds we have investigated, we find that the susceptibility data are essentially consistent with the values of n_f and Δ obtained from the spectroscopies. In a forthcoming paper,[46] we show that for values of Δ and n_f in the range of Table I, one should expect the electron-phonon coupling to lead to a similar renormalization of ϵ_f for both the calculation of the susceptibility and the valence photoemission spectrum, unless the coupling constant is very large. In Sec. IX we also discussed the lattice-parameter data and showed that these data are not necessarily in conflict with the values of n_f deduced here. It would be interesting to see if our values of n_f and Δ can be also reconciled with other low-energy experiments. For instance, the quasielastic linewidth in neutron scattering depends[47] on both n_f and Δ, and the study of this linewidth may provide further insight in the choice of parameters for the Anderson model.

ACKNOWLEDGMENTS

We would like to thank J. W. Allen, N. d'Ambrumenil A. Bringer, J. C. Fuggle, P. Fulde, G. Krill, R. M. Martin, G. A. Sawatzky, J. W. Wilkins, and D. Wohlleben for fruitful discussions.

APPENDIX A

In our basic Hamiltonian (2.1) we neglect the spin-orbit splitting of the f level. Below we discuss how the results are influenced by this approximation. We assume that the spin-orbit splitting is $\Delta\epsilon_f$ ($\Delta\epsilon_f>0$). Then there are two levels at $\epsilon_f(j=\frac{5}{2})$ and $\epsilon_f+\Delta\epsilon_f(j=\frac{7}{2})$ with the degeneracies $N_{f1}=6$ and $N_{f2}=8$, respectively. To lowest order the energy is now given by [compare Eq. (3.12)]

$$\Delta E=N_{f1}\int_{-B}^{0}\frac{|V(\epsilon)|^2}{\Delta E-\epsilon_f+\epsilon}d\epsilon+N_{f2}\int_{-B}^{0}\frac{|V(\epsilon)|^2}{\Delta E-\epsilon_f-\Delta\epsilon_f+\epsilon}d\epsilon\,. \tag{A1}$$

In Fig. 18 we show numerical results for ΔE and n_f obtained from a second-order calculation. The values of n_f are particularly interesting since $1-n_f$ largely determines the weight of the f^0 peak in the core spectrum. The solid

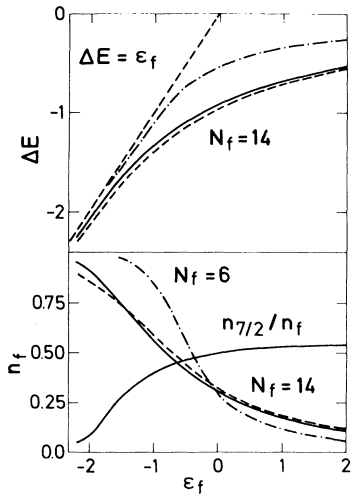

FIG. 18. Occupancy n_f and the energy lowering ΔE [Eq. (3.8)] as a function of ϵ_f. Solid curves show the results with the spin-orbit splitting included and the dashed and dashed-dotted curves have been calculated without spin-orbit splitting with $N_f=14$ and 6, respectively. The curve $n_{7/2}/n_f$ shows the occupancy of the higher ($j=\frac{7}{2}$) of the two spin-orbit-split levels divided by the total occupancy of the f level. Curve $\Delta E=\epsilon_f$ is also shown in the upper half of the figure. We have used the parameters [Eq. (3.22)] $V=0.6$, $B=6$ ($\Delta=0.12$), and $\Delta\epsilon_f=0.25$ with all energies in eV.

curves show the results when the spin-orbit splitting is taken into account. Since we expect this splitting to be of little importance for $\Delta\epsilon_f \ll |\Delta E-\epsilon_f|$, we have also performed a calculation with $\Delta\epsilon_f=0$, which amounts to using the formalism of Sec. III with $N_f=N_{f1}+N_{f2}=14$. The figure illustrates that the range of validity for this simplification is fairly large. For n_f close to one, the neglect of spin-orbit splitting, however, leads to an underestimate of n_f.

For $|\Delta E-\epsilon_f| \ll \Delta\epsilon_f$, one might expect the $j=\frac{7}{2}$ level to become unimportant. To test this assumption we have also applied the theory of Sec. III with $N_f=N_{f1}=6$. Figure 18 illustrates that this approximation actually is poor for all values of ϵ_f. For simplicity we discuss the failure of the $N_f=6$ theory in terms of the first-order theory, although the second-order correction is of importance for $N_f=6$ and $n_f\sim 1$. We introduce a quantity $\delta\equiv\epsilon_f-\Delta E$ and obtain [see Appendix C and Eq. (C6)]

$$\delta\equiv\epsilon_f-\Delta E\approx B\exp\left[\frac{\pi\epsilon_f}{N_{f1}\Delta}\right]\equiv\delta_0 \tag{A2}$$

in the limit $-\epsilon_f\gg N_{f1}\Delta/\pi$, where $n_f\approx 1$. If the $j=\frac{7}{2}$ level is included, similar arguments yield

$$\delta\approx[1+B/(\delta+\Delta\epsilon_f)]^{N_{f2}/N_{f1}}\delta_0 . \tag{A3}$$

The reason for the importance of the $j=\frac{7}{2}$ level is the logarithmic behavior of ΔE [Eqs. (A1) and (3.16)]. Thus this contribution of the $j=\frac{7}{2}$ level to ΔE is of the order

$$N_{f2}(\Delta/\pi)\ln[(\delta+\Delta\epsilon_f)/B] ,$$

which is normally important even if $\Delta\epsilon_f\gg\delta$.

In the limit $-\epsilon_f\gg N_f\Delta/\pi$ we obtain

$$1-n_f\approx\pi\delta/(N_{f1}\Delta) , \tag{A4}$$

so that the additional factor

$$[1+B/(\delta+\Delta\epsilon_f)]^{N_{f2}/N_{f1}}$$

in Fig. (A3) is crucial. This explains why the $N_f=6$ calculation is poor even when $\delta\ll\Delta\epsilon_f$.

The relative occupancy of the $j=\frac{5}{2}$ and $\frac{7}{2}$ levels is also of interest, since the $j=\frac{5}{2}$ and $\frac{7}{2}$ initial states lead to different multiplet structure and therefore different line shapes in the spectra. Figure 18 shows $n(j=\frac{7}{2})/n_f$, where $n(j=\frac{7}{2})$ is the occupancy of the $j=\frac{7}{2}$ level. For $\delta\ll\Delta\epsilon_f$, the occupancy of the $j=\frac{7}{2}$ level is very small. This can be understood from the spin-orbit-split version of Eqs. (3.13)–(3.14). In the limit $-\epsilon_f\gg N_f\Delta/\pi$, we find $\delta\ll\Delta\epsilon_f$ and

$$\frac{n(j=\frac{7}{2})}{n(j=\frac{5}{2})}\approx\frac{8}{6}\frac{\delta}{\Delta\epsilon_f+\delta}\frac{1}{1+\Delta\epsilon_f/B} . \tag{A5}$$

This result shows that although the $j=\frac{7}{2}$ level strongly influences the *total-f* occupancy via δ, the occupancy of the $j=\frac{7}{2}$ level itself is small in this limit. In the opposite limit, $\delta\gg\Delta\epsilon_f$, the occupancy is determined by the degeneracy and we obtain $n(j=\frac{7}{2})/n_f=\frac{8}{14}=0.57$. For $\epsilon_f=2$ this limit is almost reached. For Ce compounds $N_{f1}\approx N_{f2}$, and the special case $N_{f1}=N_{f2}$ is of interest. In this case it is straightforward to solve Eq. (A3) so that the spin-fluctuation limit can be treated analytically.

We now consider the effects of the spin-orbit splitting on the valence photoemission spectrum. Proceeding as in Sec. VI we derive the first-order result

$$\rho_v(\epsilon)=A^2\int d\epsilon'\,|V(\epsilon')|^2\left[\frac{N_{f1}}{(\Delta E-\epsilon_f+\epsilon')^2}+\frac{N_{f2}}{(\Delta E-\epsilon_f-\Delta\epsilon_f+\epsilon')^2}\right]\tilde{g}(z-\Delta E+\epsilon_f-\epsilon') , \tag{A6}$$

$$\tilde{g}(\epsilon)=\frac{1}{z-\epsilon_f-N_{f1}\tilde{\Gamma}(z)-N_{f2}\tilde{\Gamma}(z+\Delta\epsilon_f)} , \tag{A7}$$

where $z=\epsilon-i0^+$ and $\tilde{\Gamma}$ is defined in Eq. (6.15). In Fig. 19 we show results for both $\Delta\epsilon=0.25$ eV (solid curve) and $\Delta\epsilon_f=0$ eV (dashed curve). The solid curve has a sharp rise at ϵ_F and a shoulder about $\Delta\epsilon_f$ below ϵ_F. The rise is due to the logarithmic singularity in $N_{f1}\mathrm{Re}\tilde{\Gamma}(z)$, and the shoulder is caused by the singularity in $N_{f2}\mathrm{Re}\tilde{\Gamma}(z+\Delta\epsilon_f)$.

For $\Delta\epsilon_f=0.25$ eV we obtain $\epsilon_f-\Delta E=0.05$ eV, while $\Delta\epsilon_f=0$ leads to $\epsilon_f-\Delta E=0.12$ eV. When spin-orbit splitting is included, most of the contribution to the ϵ' integral in (A6) is therefore obtained for very small ϵ'. This explains why the introduction of spin-orbit splitting yields somewhat more weight in the neighborhood of ϵ_F. The figure, however, illustrates that spin-orbit splitting has a fairly small effect on the valence photoemission spectrum.

APPENDIX B

In Sec. III we performed a first-order ground-state calculation. Here we take double occupancy into account and extend the calculation to second order. The ground state is written as

$$|\phi_0\rangle = A\left[|0\rangle + \int_{-B}^{0} a(\epsilon)|\epsilon\rangle d\epsilon + \int_0^{B'}\left[\int_{-B}^{0} b(E,\epsilon)|E,\epsilon\rangle d\epsilon\right]dE + \int_{-B}^{0}\left[\int_{-B}^{\epsilon} c(\epsilon,\epsilon')|\epsilon,\epsilon'\rangle d\epsilon'\right]d\epsilon\right], \tag{B1}$$

where we only allow states $|\epsilon,\epsilon'\rangle$ with $\epsilon>\epsilon'$ since $|\epsilon,\epsilon'\rangle = |\epsilon',\epsilon\rangle$. Minimization of the total energy yields a set of equations analogous to Eqs. (3.9) and (3.10). Since, however, $|\epsilon,\epsilon'\rangle$ can couple to both $|\epsilon\rangle$ and $|\epsilon'\rangle$,

$$\langle\epsilon,\epsilon'|H|\epsilon''\rangle = \sqrt{N_f-1}[V(\epsilon)\delta(\epsilon'-\epsilon'')+V(\epsilon')\delta(\epsilon-\epsilon'')], \tag{B2}$$

we obtain an integral equation. To solve this equation one has to invert a matrix. Thus we define

$$B(\epsilon,\epsilon') = \left[\Delta E - \epsilon_f + \epsilon - \int_0^{B'}\frac{|V(E)|^2}{\Delta E - E + \epsilon}dE - (N_f-1)\int_{-B}^{0}\frac{|V(\epsilon'')|^2}{\Delta E - 2\epsilon_f - U + \epsilon + \epsilon''}d\epsilon''\right]$$

$$\times\delta(\epsilon-\epsilon') - (N_f-1)\frac{V(\epsilon)[V(\epsilon')]^*}{\Delta E - 2\epsilon_f - U + \epsilon + \epsilon'}, \tag{B3}$$

and obtain

$$a(\epsilon) = \sqrt{N_f}\int_{-B}^{0} B^{-1}(\epsilon,\epsilon')V(\epsilon')d\epsilon', \tag{B4}$$

$$\Delta E = N_f\int_{-B}^{0}\left[\int_{-B}^{0}[V(\epsilon)]^* B^{-1}(\epsilon,\epsilon')V(\epsilon')d\epsilon'\right]d\epsilon. \tag{B5}$$

It is now straightforward to express $b(E,\epsilon)$ and $c(\epsilon,\epsilon')$ in terms of $a(\epsilon)$,

$$b(E,\epsilon) = [V(E)]^* a(\epsilon)/(\Delta E - E + \epsilon), \tag{B6}$$

$$c(\epsilon,\epsilon') = \frac{\sqrt{N_f-1}[V(\epsilon)a(\epsilon')+V(\epsilon')a(\epsilon)]}{\Delta E - 2\epsilon_f - U + \epsilon + \epsilon'}. \tag{B7}$$

For the normalization constant A we obtain

$$A = \left[1 + \int_{-B}^{0}|a(\epsilon)|^2 d\epsilon + \int_0^{B'}\left[\int_{-B}^{0}|b(E,\epsilon)|^2 d\epsilon\right]dE + \int_{-B}^{0}d\epsilon\left[\int_{-B}^{\epsilon}d\epsilon'|c(\epsilon,\epsilon')|^2\right]\right]^{-1/2}. \tag{B8}$$

APPENDIX C

In this appendix we discuss in more detail the ground-state properties and the valence photoemission spectrum for a $V(\epsilon)$ which is constant within the band. Here we restrict ourselves to the limit $N_f\to\infty$ ($N_f\Delta$=const), where first-order theory leads to the exact results.[37] As discussed in Sec. III, one obtains for ΔE the transcendental equation

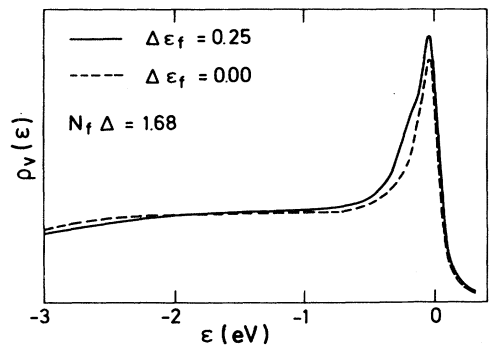

FIG. 19. Valence photoemission spectrum with (solid curve) and without (dashed curve) spin-orbit splitting. Parameters are [Eq. (3.22)] Δ=0.12 eV, B=6 eV, and $\epsilon_f=-2$ eV. We have used a constant $V(\epsilon)\equiv V$ and introduced a 0.1-eV (FWHM) Lorentzian broadening.

$$\Delta E = \frac{N_f\Delta}{\pi}\ln\left[\frac{\epsilon_f-\Delta E}{B+\epsilon_f-\Delta E}\right], \tag{C1}$$

and the occupancy of the f level is given by $n_f = C/(C+1)$, with

$$C = \frac{N_f\Delta}{\pi}\left[\frac{1}{\epsilon_f-\Delta E} - \frac{1}{\epsilon_f-\Delta E+B}\right]. \tag{C2}$$

We introduce the (positive) energy $\delta\equiv\epsilon_f-\Delta E$ and assume that the width B of the occupied part of the band is much larger than δ. Then one obtains

$$\delta = \frac{N_f\Delta}{\pi}\exp\left[\frac{\pi(\epsilon_f^*-\delta)}{N_f\Delta}\right] \tag{C3}$$

and

$$\frac{n_f}{1-n_f} = \frac{N_f\Delta}{\pi\delta}, \tag{C4}$$

with

$$\epsilon_f^* = \epsilon_f + \frac{N_f\Delta}{\pi}\ln\left[\frac{\pi B}{N_f\Delta}\right]. \tag{C5}$$

From these equations it follows that n_f is a function of *one* (dimensionless) variable $\epsilon_f^*/N_f\Delta$. This scaling

behavior was first discussed by Haldane[48] and Jefferson[49] using the "poor-man's scaling" technique. Note that this scaling behavior only holds when the bandwidth is sufficiently large ($B \gg \delta$). For $\delta \ll N_f\Delta/\pi$, i.e., $1-n_f \ll n_f$ the solution of (C3) is trivial

$$\delta = \frac{N_f\Delta}{\pi}\exp\left[\frac{\pi\epsilon_f^*}{N_f\Delta}\right] + O\left[\frac{\delta\pi}{N_f\Delta}\right] . \tag{C6}$$

In the spin-fluctuation limit, $\epsilon_f^* \ll -N_f\Delta/\pi$, where the exponent is very large and negative, δ (when divided by k_B) is called the *Kondo-temperature*. In this limit the f-level occupancy is very close to 1,

$$1-n_f \approx \exp\left[-\frac{\pi|\epsilon_f^*|}{N_f\Delta}\right] . \tag{C7}$$

Note that this result is very different in form from the exact result for $N_f=1$, which is given as $1-n_f \approx \Delta/\pi|\epsilon_f|$ if n_f is close to 1.

In Sec. VI we discussed in detail the sharp rise of the valence spectral function $\rho_v(\epsilon)$ when ϵ approaches the Fermi energy from below. We show here that the continuum contribution starting below $\epsilon_F-\delta$ does not alter this picture, which arises from the discussion of "pole contribution" (6.23) only. The complete expression for $\rho_v(\epsilon)$ for constant $V(\epsilon)$ reads

$$\rho_v(\epsilon) = \Theta(-\epsilon)(1-n_f)\frac{N_f\Delta}{\pi}\left[\frac{1-n_f}{(\epsilon-\delta)^2} + \int_{-B}^{0}\frac{1}{(\epsilon'-\delta)^2}\frac{\Theta(\epsilon'-\epsilon-\delta)N_f\Delta/\pi}{[\epsilon+\delta-\epsilon'-\epsilon_f-\mathrm{Re}\tilde{\Gamma}(\epsilon+\delta-\epsilon')]^2+(N_f\Delta)^2}d\epsilon'\right] . \tag{C8}$$

In the spin-fluctuation limit we can use (C6), (C7), and the expression for $\mathrm{Re}\tilde{\Gamma}$ for constant $V(\epsilon)$ to obtain

$$\rho_v(\epsilon) = \Theta(-\epsilon)(1-n_f)\left[\frac{\delta}{(\epsilon-\delta)^2} + \frac{\Theta(-\epsilon-\delta)}{\pi^2}\int_{\epsilon+\delta}^{0}\frac{1}{(\epsilon'-\delta)^2}\frac{1}{\left[\frac{\epsilon-\epsilon'}{N_f\Delta}+\frac{1}{\pi}\ln\frac{\epsilon+\delta-\epsilon'}{\delta}\right]^2+1}d\epsilon'\right] . \tag{C9}$$

If we measure all energies in units of δ, i.e., $\epsilon = x\delta$, we see that the term $(\epsilon-\epsilon')/N_f\Delta$ in the integrand is of order $\delta/N_f\Delta$ and can therefore be neglected in the extreme spin-fluctuation limit for $|x|$ of order 1. On the energy scale δ we then obtain a universal shape for $\rho_v(\epsilon)$ near ϵ_F,

$$\rho_v(x\delta) = \Theta(-x)\frac{\pi}{N_f\Delta}\left[\left[\frac{1}{x-1}\right]^2 + \Theta(-x-1)\int_{1+x}^{0}\frac{1}{(x'-1)^2}\frac{dx'}{[\ln(x-x')]^2+\pi^2}\right] . \tag{C10}$$

This is shown in Fig. 20. The other characteristic feature of $\rho_v(\epsilon)$ in the spin-fluctuation limit is the "normal" ionization peak at

$$\tilde{\epsilon}_f = \epsilon_f + \mathrm{Re}\tilde{\Gamma}(\tilde{\epsilon}_f) = \epsilon_f^* + (N_f\Delta/\pi)\ln[N_f\Delta/(\pi\tilde{\epsilon}_f)]$$

for $|\tilde{\epsilon}_f| \ll B$. The width of the nearly Lorentzian ionization peak is $N_f\Delta$. The value of $\rho_v(\epsilon)$ at the maximum is smaller than the value at the Fermi energy,

$$\rho_v(\tilde{\epsilon}_f)/\rho_v(\epsilon_F) \approx 1/\pi^2 . \tag{C11}$$

APPENDIX D

The general approach for calculating the core spectrum was described in Sec. IV. We now consider the case when $U=\infty$, so that double occupancy can be neglected and we can consider a first-order calculation. In this case an analytical solution can be obtained.

This limit is of practical interest for La compounds where the f^2 configuration has negligible weight, $w(f^2)$, in the initial state, and is less important in the final states than for Ce compounds. The spectrum does, however, change when double occupancy is allowed, as is illustrated in Fig. 21. For the values of U considered, $w(f^2)$ is very small ($<10^{-3}$), and the variation of the spectrum with U is due to the interaction between the final f^1 and f^2 configurations. For $U=4$ these configurations are degenerate and the interaction between them leads to final states with f^1 character over a larger energy range. Since states with f^1 character can couple to the initial state, the spectrum is indirectly influenced by the presence of the f^2 configura-

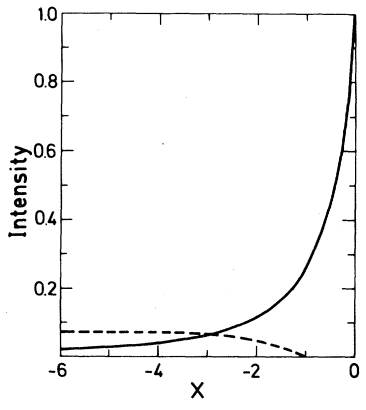

FIG. 20. Universal curve [(C10)]. Solid curve shows the pole contribution $1/(x-1)^2$ and the dashed curve shows the integral. Latter curve has a very broad maximum at about $x=-5$.

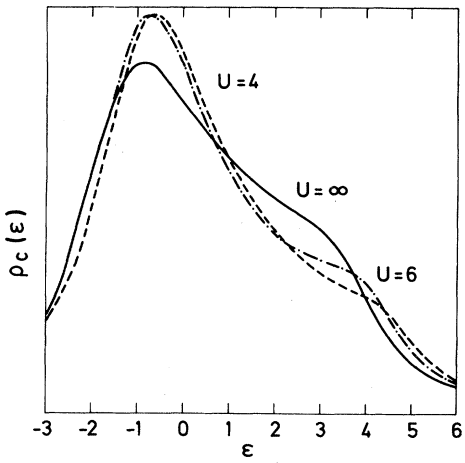

FIG. 21. Core-level spectrum as a function of U for La compounds. Solid curve shows the results when double occupancy is suppressed ($U=\infty$) and the dashed and dashed-dotted curves show the spectra for more realistic cases with $U=4$ and 6 eV, respectively. We have used the parameters [Eq. (3.22)] $\epsilon_f=5$ eV, $U_{fc}=9$ eV, $B=6$ eV, $\Delta=0.1$ eV, and $N_f=14$.

tion. In the same way we expect an influence on the Ce spectrum if the f^3 configuration is taken into account. Nevertheless, the figure illustrates that the neglect of the f^2 configuration for La compounds (and probably the neglect of the f^3 configuration for Ce compounds) should not be too serious, although it will change the values of the parameters deduced somewhat.

We need the matrix elements of $z-E_0(N)+H$ between the states $|\tilde{0}\rangle=\psi_c|0\rangle$ and $|\tilde{\epsilon}\rangle=\psi_c|\epsilon\rangle$ [Eqs. (3.1) and (3.2)], where we suppress the tilde in the following:

$$\langle 0|[z-E_0(N)+H]|0\rangle=z-\Delta E\ , \tag{D1}$$

$$\langle \epsilon|[z-E_0(N)+H]|0\rangle=\sqrt{N_f}V(\epsilon)\ , \tag{D2}$$

$$\langle \epsilon|[z-E_0(N)+H]|\epsilon'\rangle=(z-\Delta E+\epsilon_f-U_{fc}-\epsilon)\delta(\epsilon-\epsilon')\ . \tag{D3}$$

The inversion of this matrix is closely related to the calculation of the valence density of states of the nondegenerate model and we can use the same technique. We write the matrix element (D1)—(D3) in the form

$$\begin{bmatrix}[z-E_0(N)+H]_{00} & H_{01}\\ H_{10} & [z-E_0(N)+H]_{11}\end{bmatrix}\equiv\begin{bmatrix}g_{00}(z) & g_{01}(z)\\ g_{10}(z) & g_{11}(z)\end{bmatrix}^{-1}\ , \tag{D4}$$

where H_{10}, H_{01}, and H_{11} are block matrices and the index 1 refers to the states $|\epsilon\rangle$. Equation (D4) also defines the Green's functions g_{00}, g_{10}, g_{01}, and g_{11}. It is now very convenient to use the formula

$$g_{00}(z)=\{[z-E_0(N)+H]_{00}-H_{01}[z-E_0(N)+H]_{11}^{-1}H_{10}\}^{-1}\ , \tag{D5}$$

since $[z-E_0(N)+H]_{11}$ is diagonal, so that the inversion in (D5) is trivial. We shall repeatedly use a similar technique later to invert matrices which would otherwise be too large for a numerical treatment. We obtain

$$g_{00}(z)=[z-\Delta E-N_f\tilde{\Gamma}(z-\Delta E+\epsilon_f-U_{fc})]^{-1}\ , \tag{D6}$$

where

$$\tilde{\Gamma}(z)=\int_{-B}^{0}\frac{|V(\epsilon)|^2}{z-\epsilon}d\epsilon\ . \tag{D7}$$

The major difference from the calculation of the valence density of states of a nondegenerate Anderson model[19] is the limitation of the integral (D7) to states below $\epsilon_F=0$. Simple matrix algebra yields

$$g_{0\epsilon}(\epsilon)=-f(\epsilon,z)g_{00}(z)\ , \tag{D8}$$

$$g_{\epsilon\epsilon'}(z)=(z-\Delta E+\epsilon_f-U_{fc}-\epsilon)^{-1}\delta(\epsilon-\epsilon')+f(\epsilon,z)g_{00}(z)f(\epsilon',z)\ , \tag{D9}$$

where

$$f(\epsilon,z)=\sqrt{N_f}V(\epsilon)/(z-\Delta E+\epsilon_f-U_{fc}-\epsilon)\ . \tag{D10}$$

Performing the sum in Eq. (4.3) we obtain the core spectrum,

$$\rho_c(\epsilon)=\frac{A^2}{\pi}\mathrm{Im}\left[g_{00}(z)\left[1-\int a(\epsilon')f(\epsilon',z)d\epsilon'\right]^2+\int\frac{|a(\epsilon')|^2}{z-\Delta E+\epsilon_f-U_{fc}-\epsilon'}d\epsilon'\right]\ . \tag{D11}$$

This expression can be shown to be identical to the result we have obtained earlier in the nondegenerate "filled-band" model,[27]

$$\rho_c(\epsilon)=\frac{1}{\pi}\left[\frac{U_{fc}}{\epsilon-U_{fc}}\right]^2(1-n_f)\mathrm{Im}g_{00}(z)\ . \tag{D12}$$

The assumption that N_f is large allows us to neglect the conduction states above the Fermi energy (filled-band model). If in addition we assume $U\to\infty$, only the states $|0\rangle$ and $|\epsilon\rangle$ are needed. The present problem can then be mapped onto a nondegenerate filled-band model with the interaction $\sqrt{N_f}V(\epsilon)$. This justification for the filled-band model was not given in the earlier derivation,[27] and the model was only applied to the case when ϵ_f is far above the Fermi energy in the initial state.

APPENDIX E

We now describe in detail the calculation of the second-order core spectrum including double occupancy. In contrast to the calculation in Appendix D this calculation requires a numerical inversion of a matrix.

The basis functions used are defined in Eqs. (3.1)—(3.4). The ground-state calculation in this space was described in

Appendix B. To obtain core spectrum (4.3), we have to invert the matrix $\langle i \mid z-E_0(N)+H \mid j \rangle$ where $\mid i \rangle$ and $\mid j \rangle$ are the basis functions (3.1)—(3.4) with a core hole, which is not explicitly shown. Most of the relevant matrix elements have been given in Eqs. (3.11), (3.21), and (B2). Following the notation in Eq. (B1) the Hamiltonian matrix is written in the block form as follows:

$$\begin{bmatrix} H_{00} & H_{0a} & 0 & 0 \\ H_{a0} & H_{aa} & H_{ab} & H_{ac} \\ 0 & H_{ba} & H_{bb} & 0 \\ 0 & H_{ca} & 0 & H_{cc} \end{bmatrix} , \tag{E1}$$

where 0, a, b, and c refer to the states $\mid 0 \rangle$, $\mid \epsilon \rangle$, $\mid E\epsilon \rangle$, and $\mid \epsilon\epsilon' \rangle$, respectively. All the elements in matrix (E1) are block matrices except for the c number H_{00}. Matrix (E1) is too large to be readily inverted numerically. For instance, matrix H_{bb} has a double-continuum index $E\epsilon$. Thus we proceed in a way similar to Eq. (D5) and calculate

$$\begin{bmatrix} G_{00} & G_{0a} \\ G_{a0} & G_{aa} \end{bmatrix} = \begin{bmatrix} H_{00} & H_{0a} \\ H_{a0} & \tilde{H}_{aa} \end{bmatrix}^{-1} , \tag{E2}$$

where

$$\tilde{H}_{aa} = H_{aa} - H_{ab} H_{bb}^{-1} H_{ba} - H_{ac} H_{cc}^{-1} H_{ca} . \tag{E3}$$

To invert this matrix we discretize the energy mesh and introduce N equidistant points ϵ_i in the energy range $(-B,0)$ with an energy step $\Delta\epsilon$. We define weight factors w_i according to some integration method. Simpson's method, for instance, gives the values $\Delta\epsilon/3$, $2\Delta\epsilon/3$, and $4\Delta\epsilon/3$ for the w_i's. With the use of the index 0 for the function $\mid 0 \rangle$ and $i=1,\ldots,N$ for the functions $\mid \epsilon_i \rangle$, the matrix elements in (E2) and (E3) are given by

$$H_{00} = z - \Delta E , \tag{E4}$$

$$H_{0i} = \sqrt{N_f}[V(\epsilon_i)]^* \sqrt{\omega_i} , \tag{E5}$$

$$\tilde{H}_{ij} = [z - \Delta E + \epsilon_f - U_{fc} - \epsilon_i - (N_f - 1)\tilde{\Gamma}(z - \Delta E + 2\epsilon_f - 2U_{fc} + U - \epsilon_i) - \gamma(z - \Delta E - \epsilon_i)]\delta_{ij} - (N_f - 1)\frac{[V(\epsilon_i)]^* V(\epsilon_j)\sqrt{w_i w_j}}{z - \Delta E + 2\epsilon_f - 2U_{fc} + U - \epsilon_i - \epsilon_j} , \tag{E6}$$

where $\tilde{\Gamma}$ was defined in Eq. (D7) and

$$\gamma(z) = \int_0^{B'} \frac{\mid V(E) \mid^2}{z + E} dE . \tag{E7}$$

To obtain the remaining elements of the Green's function we now use formulas of the type

$$G_{ba} = -H_{bb}^{-1} H_{ba} G_{aa} , \tag{E8}$$

$$G_{bb} = H_{bb}^{-1} + H_{bb}^{-1} H_{ba} G_{aa} H_{ab} H_{bb}^{-1} . \tag{E9}$$

According to Eq. (4.3) these Green's-function matrices are multiplied by the coefficients a, b, and c in (B1). Since b and c are expressed in terms of a in Eqs. (B6) and (B7), we do not need to explicitly calculate b and c or matrices (E8) and (E9). For instance, we define

$$b_{\nu i} \equiv \sqrt{w_\nu} b(E_\nu, \epsilon_i) \sqrt{w_i} , \tag{E10}$$

and obtain

$$\sum_{\nu,i} b_{\nu i} (G_{ba})_{\nu i, j} = -\sum_i \sum_\nu \frac{w_\nu \mid V(E_\nu) \mid^2 a(\epsilon_i) \sqrt{w_i} (G_{aa})_{ij}}{(\Delta E - E_\nu + \epsilon_i)(z - \Delta E + E_\nu - \epsilon_i)} . \tag{E11}$$

Thus we introduce

$$f_i = \int_0^{B'} \frac{\mid V(E) \mid^2}{(\Delta E - E + \epsilon_i)(z - \Delta E + E - \epsilon_i)} dE , \tag{E12}$$

which can be expressed in terms of γ [Eq. (E7)],

$$f_i = \frac{1}{z}[\gamma(z - \Delta E - \epsilon_i) - \gamma(-\Delta E - \epsilon_i)] . \tag{E13}$$

Similarly, we define

$$h_i = A(N_f - 1)\sqrt{w_i} \int_{-B}^{0} \frac{\mid V(\epsilon) \mid^2 a(\epsilon_i) + V(\epsilon) V(\epsilon_i) a(\epsilon)}{(\Delta E - 2\epsilon_f - U + \epsilon + \epsilon_i)(z - \Delta E + 2\epsilon_f - 2U_{fc} + U - \epsilon - \epsilon_i)} d\epsilon \tag{E14}$$

to take the coefficients $c(\epsilon,\epsilon')$ into account. Finally we define

$$a_0 = A , \tag{E15}$$

$$a_i = A a(\epsilon_i) \sqrt{w_i}, \quad i = 1, \ldots, N \tag{E16}$$

and denote matrix (E2) by G_{ij}, where indices i and j run from 0 to N. The spectrum is then given by

$$p_c(\epsilon)=\frac{1}{\pi}\mathrm{Im}\left[\sum_{i=0}^{N}\sum_{j=0}^{N}k_iG_{ij}k_j+A^2\int_0^{B'}dE\int_{-B}^{0}d\epsilon\frac{|b(E,\epsilon)|^2}{z-\Delta E+E-\epsilon}\right.$$
$$\left.+A^2\int_{-B}^{0}d\epsilon\int_{-B}^{\epsilon}d\epsilon'\frac{|c(\epsilon,\epsilon')|^2}{z-\Delta E+2\epsilon_f-2U_{fc}+U-\epsilon-\epsilon'}\right], \quad \text{(E17)}$$

where $z=\epsilon-i0^+$, $k_i=(1-f_i)a_i-h_i$, and $h_0=f_0=0$.

APPENDIX F

Many Ce compounds have a magnetic ground state while all the calculations in this paper were for a singlet ground state. Since our basic Hamiltonian (2.1) cannot have a magnetic ground state,[50] we must go beyond the impurity model to discuss the magnetic Ce compounds. An accurate treatment of the Anderson lattice model is, however, not within scope of this paper. Instead we use a mean-field-type approach and add an additional term

$$\epsilon_M\sum_{\nu}n_\nu\langle n_\nu\rangle \quad \text{(F1)}$$

to (2.4). This term is supposed to describe a tendency for the spins to order ferromagnetically. Whether the ground state is ferromagnetic or not depends on the size of ϵ_M and $N_f|V(\epsilon)|^2$. We assume that ϵ_M is large enough to give a ferromagnetic ground state with the state $|\nu\rangle$ preferentially occupied. This leads to two effective levels,

$$\epsilon_{f1}=\epsilon_f+\epsilon_M\langle n_\nu\rangle\ , \quad \text{(F2)}$$

$$\epsilon_{f2}=\epsilon_f+\epsilon_M\sum_{\nu'\neq\nu}\langle n_{\nu'}\rangle/(N_f-1)\ . \quad \text{(F3)}$$

We can now use the formalism of Appendix A and make the identification $N_{f1}=1$, $N_{f2}=N_f-1$, $\Delta\epsilon_f=\epsilon_{f2}-\epsilon_{f1}$, and $\epsilon_f=\epsilon_{f1}$.

In Fig. 22 we show spectra calculated this way. The solid curve shows results for a magnetic ground state where one n_ν is larger than the others. The dashed curve is for a nonmagnetic state where all n_ν were kept equal. The magnetic solution gave $\Delta E=-1.982$ eV, $\epsilon_{f1}=-1.979$ eV, $\epsilon_{f2}=-1.602$ eV, and $n_f=0.976$. The large occupancy is mainly due to the preferred level, which is almost full ($n_\nu=0.949$). The nonmagnetic state has a higher energy ($\Delta E=-1.85$ eV) and a substantially lower f occupancy ($n_f=0.72$). To understand the large difference in n_f between the magnetic and nonmagnetic states we apply formulas (A2)—(A4), although $V(\epsilon)$ is not sufficiently small in this example to make the formulas very accurate. For the nonmagnetic solution we obtain

$$1-(n_f)_{\mathrm{nonmag}}=\frac{\pi B}{N_f\Delta}\exp\left[\frac{\pi\epsilon_f}{N_f\Delta}\right], \quad \text{(F4)}$$

and for the magnetic solution we find

$$1-(n_f)_{\mathrm{mag}}\approx\frac{\pi B}{\Delta}\left[\frac{B}{\epsilon_{f2}-\epsilon_{f1}}\right]^{(N_f-1)}\exp\left[\frac{\pi\epsilon_f}{\Delta}\right]. \quad \text{(F5)}$$

Although the prefactors are quite different the decisive difference is the appearance of $N_f\Delta$ in the exponent of (F4) but only Δ in (F5). Since ϵ_f is negative the value of the exponential function in (F5) is normally extremely small. The reason is that the hopping between the f level and the conduction states is governed by $N_f\Delta$ for the nonmagnetic state where all the levels ν are equally occupied, and by Δ for the magnetic state, where one level ν is preferentially occupied. We can therefore not automatically infer that Δ is small from the observation that $n_f\sim1$ for a magnetic state.

Figure 22 shows that both the magnetic and nonmagnetic states lead to a peak close to ϵ_F. The magnetic state leads to a peak slightly below ϵ_F which is mainly due to a structure in $(N_f-1)\tilde{\Gamma}$ in Eq. (A7). This peak corresponds to final states similar to the *nonmagnetic* state but with a conduction electron close to ϵ_F removed. Since these final states have higher energies than the *magnetic* ground state the peak is located below ϵ_F. It is very important that this structure is governed by $(N_f-1)\Delta$ and not Δ. This is related to the fact that the final states are nonmagnetic. There is a much weaker structure at ϵ_F (not visible in the figure) corresponding to a magnetic final state and determined by Δ. Since the stronger peak is related to the strength of $(N_f-1)\Delta$, we expect the weight close to ϵ_F to be comparable for the magnetic and the nonmagnetic states. Actually there is even somewhat more weight at ϵ_F for the magnetic state. The main reason is the small value of $\epsilon_{f1}-\Delta E$, which means that most of the contribution to the ϵ' integral in Eq. (A6) comes very close to $\epsilon'=0$. The peak in $\tilde{g}(\epsilon)$ [Eq. (A7)] is therefore spread out very little in the ϵ' integration.

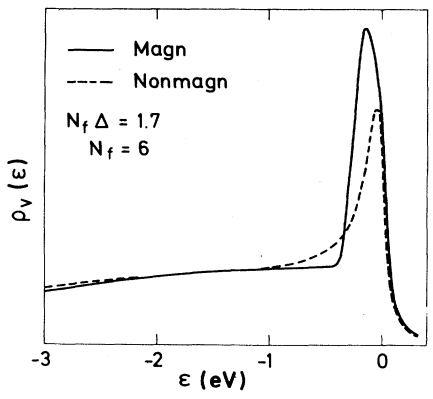

FIG. 22. Valence photoemission spectrum for a magnetic (solid curve) and a nonmagnetic (dashed curve) initial state. We used the parameters $\epsilon_f=-1.6$ eV, $B=6$ eV, and $\epsilon_M=-0.4$ eV, and assumed a constant $V(\epsilon)\equiv V$. Lorentzian broadening of 0.1 eV (FWHM) was used.

[1]See, e.g., J. M. Lawrence, P. S. Riseborough, and R. D. Parks Rep. Prog. Phys. 41, 1 (1981), for a review and further references.

[2]*Valence Fluctuations in Solids,* edited by L. M. Falicov, W. Hanke, and M. P. Maple, (North-Holland, Amsterdam, 1981).

[3]*Valence Instabilities,* edited by P. Wachter and H. Boppart (North-Holland, Amsterdam, 1982).

[4]D. M. Newns and A. C. Hewson, J. Phys. F 10, 2429 (1980); in *Valence Fluctuations in Solids,* Ref. 2, p. 27.

[5]A. Iandelli and A. Palenzona, in *Handbook on the Physics and Chemistry of Rare Earths,* edited by K. A. Geschneidner and L. Eyring (North-Holland, Amsterdam, 1979), Vol. II, p. 1.

[6]See, however B. Johansson, Philos. Mag. 30, 469 (1974), for different conclusions.

[7]See, e.g., M. Campagna, G. K. Wertheim, and Y. Baer, in *Photoemission in Solids II,* edited by L. Ley and M. Cardona (Springer, Berlin, 1977), p. 217, and references therein; Y. Baer and Ch. Zürcher, Phys. Rev. Lett. 39, 956 (1977); Y. Baer, R. Hauger, Ch. Zürcher, M. Campagna, and G. K. Wertheim, Phys. Rev. B 18, 4433 (1978); G. Crecelius, G. K. Wertheim, and D. N. E. Buchanan, Phys. Rev. B 18, 6519 (1978).

[8]G. Krill, L. Abadli, M. F. Ravet, J. P. Kappler, and A. Meyer, J. Phys. (Paris) 41, 1121 (1980); G. Krill, J. P. Kappler, M. F. Ravet, A. Amamou, and A. Meyer, J. Phys. F 10, 1031 (1980); G. Krill, J. P. Kappler, A. Meyer, L. Abadli, and M. F. Ravet, J. Phys. F 11, 1713 (1981); L. C. Gupta, E. V. Sampathkumaran, R. Vijayaraghavan, M. S. Hedge, and C. N. R. Rao, J. Phys. C 13, L455 (1980).

[9]J. C. Fuggle, M. Campagna, Z. Zołnierek, and R. Lässer, Phys. Rev. Lett. 45, 1597 (1980); F. U. Hillebrecht, and J. C. Fuggle, Phys. Rev. B 25, 3550 (1982); J. C. Fuggle, F. U. Hillebrecht, Z. Zołnierek, Ch. Freiburg, and M. Campagna, in *Valence Instabilities,* Ref. 3, p. 267.

[10]See S. Hüfner and P. Steiner, Z. Phys. B 46, 37 (1982), for references to, and a discussion of, core-level XPS as well as valence photoemission; P. Steiner, H. Höchst and S. Hüfner, J. Phys. F 7, L145 (1977).

[11]J. W. Allen, S.-J. Oh, I. Lindau, J. M. Lawrence, L. I. Johansson, and S. B. Hagström, Phys. Rev. Lett. 46, 1100 (1981); M. Croft, J. H. Weaver, D. J. Peterman, and A. Franciosi, Phys. Rev. Lett. 46, 1104 (1981).

[12]M. Croft, A. Franciosi, J. H. Weaver, and A. Jayaraman, Phys. Rev. B 24, 544 (1981); A. Franciosi, J. H. Weaver, N. Mårtensson, and M. Croft, Phys. Rev. B 24, 3651 (1981); N. Mårtensson, B. Reihl, and R. D. Parks, Solid State Commun. 41, 573 (1982); W. Gudat, M. Iwan, R. Pinchaux, and F. Hullinger, in *Valence Instabilities,* Ref. 3, p. 249; D. Wieliczka, J. M. Weaver, D. W. Lynch, and C. G. Olson, Phys. Rev. B 26, 7056 (1982); F. Gerken, J. Barth, and C. Kunz, in *X-Ray and Atomic Inner-Shell Physics—1982 (International Conference, University of Oregon),* edited by B. Crasemann (AIP, New York, 1982), p. 602.

[13]J. W. Allen, S.-J. Oh, I. Lindau, M. P. Malpe, J. F. Suassuna, and S. B. Hagström, Phys. Rev. B 26, 445 (1982); J. M. Lawrence, J. W. Allen, S.-J. Oh, and I. Lindau, Phys. Rev. B 26, 2362 (1982).

[14]H. Launois, M. Rawiso, E. Holland-Moritz, R. Pott, and D. Wohlleben, Phys. Rev. Lett. 44, 1271 (1980); R. M. Martin, J. B. Boyce, J. W. Allen, and F. Holzberg, Phys. Rev. Lett. 44, 1275 (1980).

[15]D. K. Wohlleben, in *Valence Fluctuations in Solids,* Ref. 2, p. 1; K. R. Bauchspiess, W. Boksch, E. Holland-Moritz, H. Launois, R. Pott, and D. Wohllenben, in *Valence Fluctuations in Solids,* Ref. 2, p. 417.

[16]J. K. Lang, Y. Baer, and P. A. Cox, Phys. Rev. Lett. 42, 74 (1978); P. A. Cox, J. K. Lang, and Y. Baer, J. Phys. F 11, 113 (1981); J. K. Lang, Y. Baer, and P. A. Cox, J. Phys. F 11, 121 (1981); Y. Baer, H. R. Ott, J. C. Fuggle, and L. E. DeLong, Phys. Rev. B 24, 5384 (1981).

[17]U. Kornstädt, R. Lässer, and B. Lengeler, Phys. Rev. B 21, 1898 (1980).

[18]D. R. Gustafson, J. D. McNutt, and L. O. Roellig, Phys. Rev. 183, 435 (1969); R. F. Gempel, D. R. Gustafson, and J. D. Willenberg, Phys. Rev. B 5, 2082 (1972).

[19]P. W. Anderson, Phys. Rev. 124, 41 (1961).

[20]J. C. Fuggle, F. U. Hillebrecht, J.-M. Esteva, R. C. Karnatak, O. Gunnarsson, and K. Schönhammer, Phys. Rev. B 27, 4637 (1983).

[21]J. C. Fuggle, F. U. Hillebrecht, Z. Zołnierek, R. Lässer, Ch. Freiburg, O. Gunnarsson, and K. Schönhammer, Phys. Rev. B 27, 7330 (1983).

[22]F. U. Hillebrecht, J. C. Fuggle, G. A. Sawatzky, O. Gunnarsson, and K. Schönhammer (unpublished).

[23]O. Gunnarsson, K. Schönhammer, J. C. Fuggle, F. U. Hillebrecht, J.-M. Esteva, R. C. Karnatak, and B. Hillebrand (unpublished).

[24]J. F. Herbst and J. W. Wilkins, Phys. Rev. Lett. 43, 1760 (1979); J. F. Herbst, R. E. Watson, and J. W. Wilkins, Phys. Rev. B 13, 1439 (1976); B 17, 3089 (1978).

[25]B. Johansson and N. Mårtensson, Phys. Rev. B 24, 4484 (1981).

[26]A. Kotani and Y. Toyozawa, J. Phys. Soc. Jpn. 35, 1073 (1973); 37, 912 (1974); 46, 488 (1979); J. W. Gadzuk and S. Doniach, Surf. Sci. 77, 427 (1978); S. S. Hussein and D. M. Newns, Solid State Commun. 25, 1049 (1978).

[27]K. Schönhammer and O. Gunnarsson, Solid State Commun. 23, 691 (1977); 26, 399 (1978); Phys. Rev. B 18, 6606 (1978); Z. Phys. B 30, 297 (1978); O. Gunnarsson and K. Schönhammer, Solid State Commun. 26, 147 (1978); Phys. Rev. Lett. 41, 1608 (1978).

[28]D. A. Shirley, Chem. Phys. Lett. 16, 220 (1972); N. D. Lang and A. R. Williams, Phys. Rev. B 16, 2408 (1977).

[29]P. Nozières and C. T. DeDominicis, Phys. Rev. 178, 1097 (1969).

[30]S.-J. Oh and S. Doniach, Phys. Rev. B 26, 2085 (1982).

[31]T. V. Ramakrishnan, in *Valence Fluctuations in Solids,* Ref. 2, p. 13; T. V. Ramakrishnan and K. Sur, Phys. Rev. B 26, 1798 (1982); P. W. Anderson, in *Valence Fluctuations in Solids,* Ref. 2, p. 451.

[32]For calculations of the f level Green's function, see also P. Schlottmann, Phys. Status Solidi 111, 161 (1982); N. Grewe and H. Keiter, Phys. Rev. B 24, 4420 (1981).

[33]J. W. Allen and R. P. Martin, Phys. Rev. Lett. 49, 1106 (1982).

[34]O. Gunnarsson and K. Schönhammer, Phys. Rev. Lett. 50, 604 (1983).

[35]A. Bringer and H. Lustfeld, Z. Phys. B 28, 213 (1977); H. Lustfeld, and A. Bringer, Solid State Commun. 28, 119 (1978).

[36]C. M. Varma and Y. Yafet, Phys. Rev. B 13, 2950 (1976).

[37]Strictly speaking, the arguments about exactness in the limit $N_f \to \infty$ are correct only for an arbitrary large but finite system.

[38]K. Yamada, Prog. Theor. Phys. 53, 970 (1975).

[39]R. M. Martin, Phys. Rev. Lett. 48, 362 (1982).

[40]D. C. Langreth, Phys. Rev. 150, 516 (1966); F. D. M. Haldane, in *Valence Fluctuations in Solids,* Ref. 2, p. 153; R. M. Martin and J. W. Allen, in *Valence Fluctuations in Solids,* Ref. 2, p. 85; A. Yoshimori and A. Zawadowski, J. Phys. C 15, 5241 (1982).

[41]M. E. Rose, *Elementary Theory of Angular Momentum* (Wiley, New York, 1967).

[42]O. K. Andersen, Phys. Rev. B 12, 3060 (1975).

[43]G. L. Olcese, J. Phys. (Paris) C 5, 334 (1979).

[44]C. Bonnelle, R. C. Karnatak, and J. Sugar, Phys. Rev. A 9, 1920 (1974).

[45]We have not tried to subtract the fairly large contributions to χ which are not due to the f electrons because of the fairly large uncertainties in this procedure. We note, however, that even an error by a factor of 2 in our estimate of the f susceptibility would only change $w(f^0)$ by about 0.1 (see Fig. 17).

[46]K. Schönhammer and O. Gunnarsson (unpublished).

[47]Y. Kuramoto and E. Müller-Hartmann, in *Valence Fluctuations in Solids,* Ref. 2, p. 139.

[48]F. D. M. Haldane, Phys. Rev. Lett. 40, 416 (1978).

[49]J. H. Jefferson, J. Phys. C 10, 3589 (1977).

[50]A calculation based on the magnetic basis states $\psi_\nu^\dagger|0\rangle$ and $\psi_{E\nu}^\dagger|0\rangle$ for a fixed ν can give a lower energy than Eq. (3.12) for a finite N_f and $-\epsilon_f \gg \epsilon_F$. Such a calculation, however, contains contributions to the energy of the order $1/N_f$, while Eq. (3.12) is only correct to order N_f^0. A consistent inclusion of all terms of the order $1/N_f$ leads to a lower energy for the singlet state.